HIGH FIELD MAGNETORESISTANCE OF SEMICONDUCTING DIAMOND

by

KENNETH JESS RUSSELL

Bachelor of Science

Oklahoma State University

Stillwater, Oklahoma

1959

Submitted to the Faculty of the Graduate School of
the Oklahoma State University
in partial fulfillment of the requirements
for the degree of
DOCTOR OF PHILOSOPHY
August, 1965

OKLAHOMA
STATE UNIVERSITY
LIBRARY

NOV 24 1965

HIGH FIELD MAGNETORESISTANCE OF

SEMICONDUCTING DIAMOND

Thesis Approved:

William J. Lewis
Thesis Adviser

H Harrington

Louis P. Vogel

Francis C. Todd

E E Kolumbus

J H Boggs
Dean of the Graduate School

592655

ACKNOWLEDGMENTS

I am indebted to many people for aid in carrying out this study. In particular I would like to thank my advisor, Dr. W. J. Leivo, for his patience and guidance, Dr. H. E. Harrington, Chairman of the Physics Department, for aid in obtaining some of the equipment necessary for this study, and my advisory committee for their time and interest.

I would also like to acknowledge indebtedness to the Physics and Chemistry Shop personnel who made the pulse magnets and much of the hardware used in the construction of the capacitor bank.

TABLE OF CONTENTS

LIST OF TABLES

LIST OF FIGURES

CHAPTER I

THE PROBLEM

Statement of the Problem

The purpose of this investigation was to study the magnetoresistance effect in semiconducting diamond in both low and high magnetic fields. Both longitudinal and transverse effects were studied. Measurement of these effects were mainly carried out at magnetic field strengths significantly higher than those previously used to study magnetoresistance in diamond. The results of these experiments were compared with existing theories of magnetoresistance.

Limitations of the Experiment

The theory applied to the results of this experiment assumes the diamond to be homogeneous. However, as will be noted later, the sample is markedly inhomogeneous. The theory also assumes that the potential contacts do not disturb the electric field in the sample. In practice they always do by shorting a small region of the surface of the sample since they are of finite size, or by loading the surface, considering the surface as a power source (1). Placement of the contacts is also important; if they are located too near the edge of the sample the gross behavior of the potential in a magnetic field may be due to the contacts and not to the magnetoresistance effect (2). Some sources of error, e.g., the Nernst, and Righi-Leduc effects, can be eliminated by proper

experimental procedure, while others, e.g., contact errors and sample inhomogeneity, can be treated only in a general manner.

CHAPTER II

REVIEW OF THE LITERATURE

Historical Background

The first observation of magnetoresistance, the change of the electrical resistivity of a conductor brought about by application of an external magnetic field, was made over one hundred years ago, in 1856, by Sir William Thomson (3). He found that the resistance of iron was increased when a longitudinal magnetic field was applied. Magnetoresistance in electrolytes was first observed by Neesen (4) who observed the effect in iron sulphate. Boltzmann (5), in 1887, first noticed the magnetoresistance effect in gases; he observed that a magnetic field hindered the discharge in a Geissler tube and that the current was reduced as if the resistance had been increased ten times. Drude and Nernst (6), in 1891, observed magnetoresistance in liquid mercury and molten bismuth. Magnetoresistance in a Bunsen flame was investigated by Wilson (7) in 1909. The transverse magnetoresistance effect in graphite was studied in 1910 by Laws (8). In 1915 Königsberger and Gottstein (9) measured the transverse magnetoresistance effect in silicon. Kapitza (10), in 1927, made magnetoresistance measurements in solids and at high magnetic fields, previously unattainable, by using pulsed magnets.

This list of early magnetoresistance experiments is by no means complete (L. L. Campbell (11) lists many more) but was picked to show

the tremendous variation in materials in which magnetoresistance has been studied. Since these early experiments the magnetoresistance effect has been given much study, especially in metals and semiconductors and using both steady state and pulsed magnetic fields.

Previous Magnetoresistance Studies in Diamond

The first report of magnetoresistance in semiconducting diamond was made by P. T. Wedepohl (12). This was a preliminary report of an investigation that was later reported more fully by E. W. J. Mitchell and P. T. Wedepohl (13). They reported that the transverse magnetoresistance in their specimen was in reasonable agreement with the relation

$$\frac{\Delta R}{R_o} = 3.54 \times 10^{-10} H^2$$

out to the maximum magnetic field that they used which was about 4000 gauss. They also made a measurement of the magnetoresistance as a function of angle between electric and magnetic field vectors for a constant magnetic field of 3630 gauss. They then compared their results to simple low-field magnetoresistance theory, a presentation of which is given by G. L. Pearson and H. Suhl (14). They also found that the longitudinal magnetoresistance was about one-third of the transverse magnetoresistance. The next report of the observation of magnetoresistance in semiconducting diamond was made by R. T. Bate and R. K. Willardson (15). They studied transverse magnetoresistance at magnetic fields up to 20,000 gauss for temperatures between $0^{\circ}C$ and $100^{\circ}C$ and found that the transverse magnetoresistance is proportional to H^2 at low magnetic fields but deviates from this behavior for magnetic fields above 4000 gauss. The most recent work on magnetoresistance in semiconducting diamond was done by P. J. Kemmey and

E. W. J. Mitchell (16). They found the ratio $\frac{\Delta R}{R_o H^2}$ to be 2.66×10^{-10}, 2.1×10^{-10} and 1.32×10^{-10} for the longitudinal effects in [110], [100], and [111] directions respectively, and the ratio ranged from 2.79×10^{-10} to 6.8×10^{-10} for the various transverse effects. The magnetic field strengths used were less than 3600 gauss. Magnetoresistance as a function of angle between the electric and magnetic field vectors was also studied. The authors used the results of their experiments to determine the components of the magnetoconductive tensor and to compare with calculations carried out for a triply degenerate valance band, assuming that the energy surfaces can be approximated by two warped spheres and one sphere.

Summary of the Literature

Previous studies of magnetoresistance in diamond have been studies using dc magnetic fields of a relatively low value (less than about 20,000 gauss). Longitudinal and transverse magnetoresistance effects as well as magnetoresistance as a function of angle between the electric and magnetic field vectors for different orientations of the samples were studied. The results of these experiments were compared to existing low magnetic field magnetoresistance theory. The most recent work compared the results to the low magnetic field magnetoresistance theory applied to the case of a triply degenerate valance band, assuming the energy surfaces can be approximated by two warped spheres and one sphere (16).

Magnetoresistance has been studied in much higher magnetic fields in other materials by using a pulse technique to produce the higher magnetic fields (10, 17, 18). Also, recently, the magnetoresistance theory has been extended to include certain cases of arbitrary magnetic

field strengths in addition to the usual limiting cases of very weak or very strong magnetic fields (19).

CHAPTER III

DESCRIPTION OF APPARATUS

The Pulsed Magnet System

A pulsed magnet system was constructed to obtain large magnetic fields for the study of magnetoresistance in diamond. It provides stored energy of up to 45 kilojoules for producing the magnetic fields. Using systems of this type magnetic fields of 920,000 gauss have been recorded by other workers (20).

The high magnetic fields are obtained by discharging a bank of capacitors through an electromagnet. Several different magnets have been tested each of which fall into one of the three following classes: 1) The magnet coil is constructed of a beryllium copper alloy and is in the form of a continuous helix turned out of a solid bar. The magnet coil is clamped between two thick endplates, and, to further enhance the strength, the space around the coil between the endplates is filled with a cement (epoxy, Sauereisen or calcium aluminate). Others have described similar magnets (21). This type of construction gives the highest magnetic field of the three classes. An example of the magnet is shown in Fig. 1. 2) The magnet is of the flux concentrator type and has its primary winding embedded in the brass flux concentrator body which is shaped to enhance the field at the center. This method of construction has been described elsewhere and is between the first and third types in

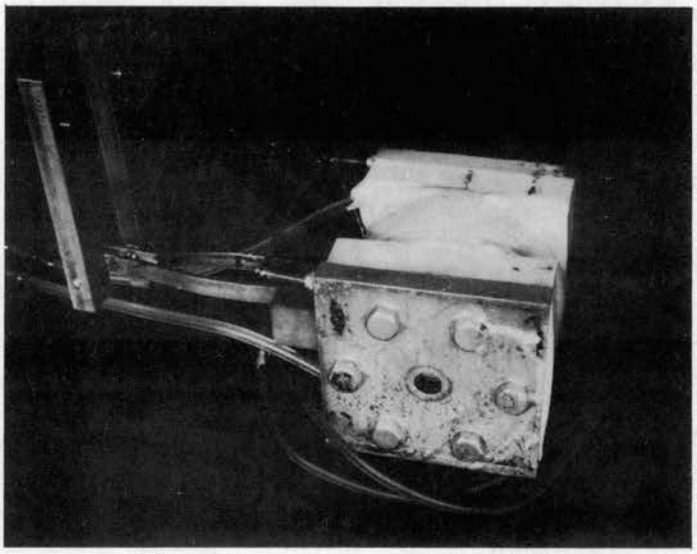

Fig. 1 Helical Coil Magnet

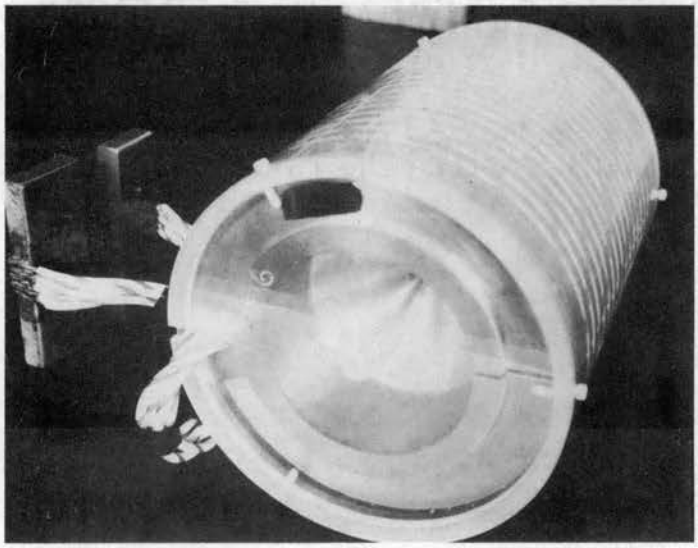

Fig. 2 Flux Concentrator Magnet

magnetic field strength (22). An example of this magnet is shown in Fig. 2. 3) The magnet coil is a multilayer coil of wire wound on an insulating mandrel. The wires are held in place by being coated with an epoxy cement during the winding process and by wrapping several layers of epoxy impregnated fiberglass material around the coil. This magnet gives the lowest magnetic field of the three types but may be desirable since it can easily be made to give very long period discharges. The high magnetic field magnetoresistance measurements were made with this type of magnet. An example of a wire wound magnet is shown in Fig. 3.

Measurement of the pulsed magnetic fields was accomplished by inserting a search coil in the magnetic field and connecting the resulting signal to an integrating circuit. The output of the integrator is displayed on an oscilloscope screen to give the variation of magnetic field with time. A Tektronix Type 551 Dual-Trace Oscilloscope with a Type O Plug-in Unit (connected as an integrator) was used in the measurement.

Figure 4 shows a block diagram of the capacitive energy storage system. The system is composed of the capacitor bank together with associated charging and switching circuits. To produce a magnetic field the capacitor bank is charged to the desired difference in potential and then discharged into the load. With the crowbar circuit inoperative, the resulting discharge current through the electromagnet will have the time variation shown in Fig. 5a. The crowbar circuit is used to limit the energy dissipated in the magnet since the resulting heating may be objectionable because of sample heating or magnet deterioration. The current pulse is limited by closing the crowbar switch at point A on the curve, Fig. 5a, and the resulting time variation of the current is essentially as shown in Fig. 5b.

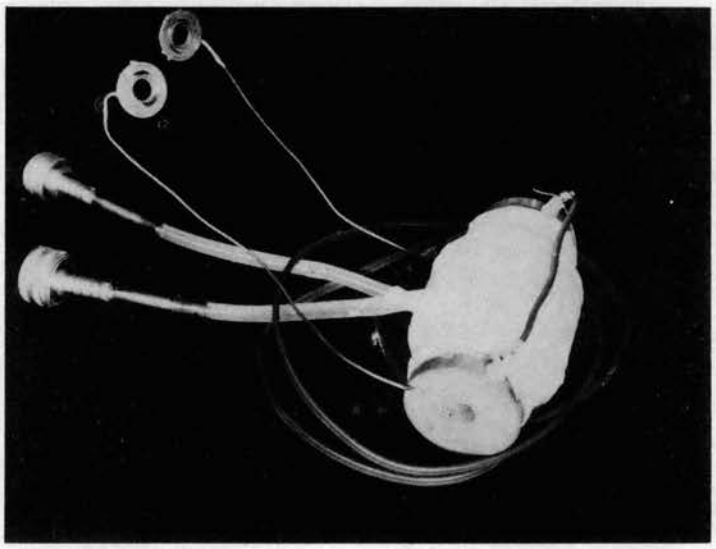

Fig. 3 Wire Wound Magnet

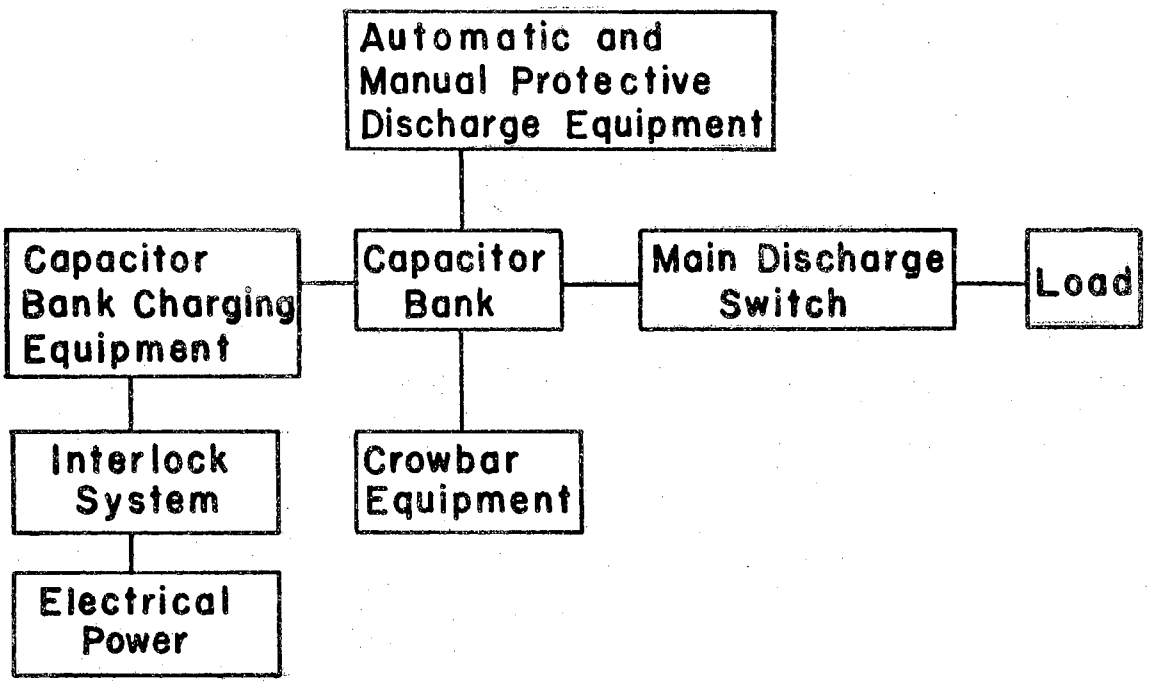

Fig. 4 Block Diagram of Pulsed Magnet System

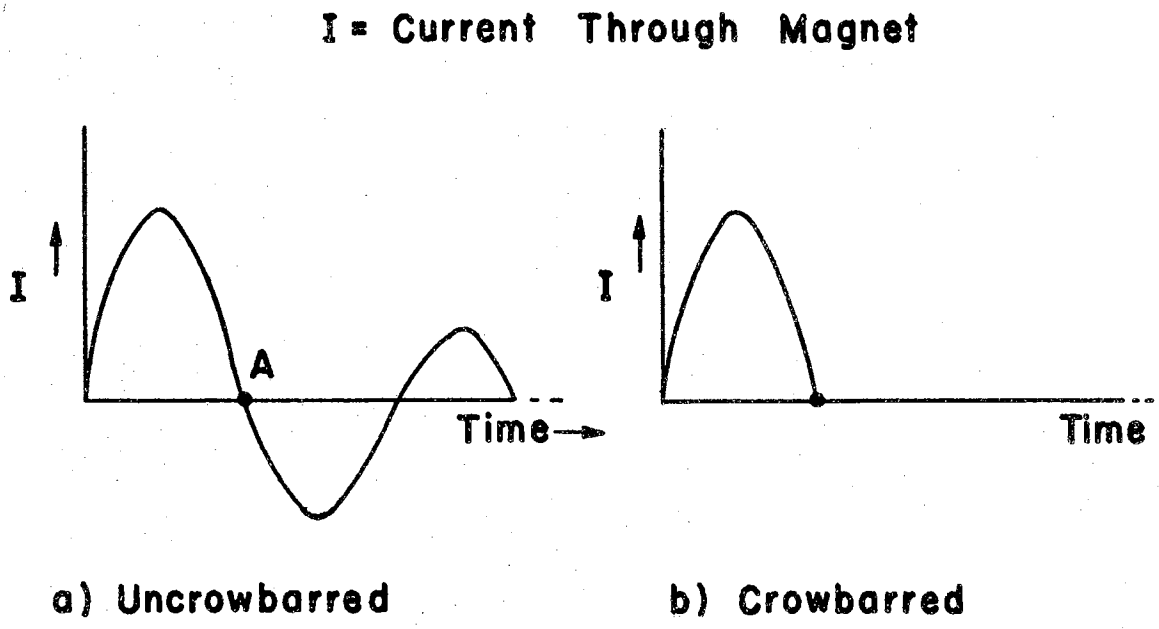

Fig. 5 Magnet Current Versus Time

To more fully describe the capacitive energy storage system consider it to be divided into four parts: 1) bank circuit, 2) bank charging circuit, 3) crowbar circuit, 4) sequence control circuit.

Let us consider first the bank circuit illustrated in Fig. 6. The capacitor bank is composed of fourteen energy storage capacitors of extended foil construction connected so that they may be discharged in parallel. The capacitors are 180 microfarad, 6000 volt units, which, in parallel, give a total capacitance of 2520 microfarads and a total stored energy of 45,360 joules. The equivalent series inductance of each capacitor is less than one microhenry, allowing efficient use of the bank with small inductances. Fourteen ignitrons, V_4 through V_{17}, one mounted on top of each capacitor, discharge the capacitor bank into the load. The simultaneous firing of the 14 ignitrons is accomplished by the discharge of the small energy storage capacitor, C_3, through the ignitors of the 14 ignitrons. This discharge is brought about by another ignitron, V_3, mounted on top of C_3. The ignitron, V_3, is fired by the hydrogen thyratron, V_2, discharging the trigger capacitor, C_3, through the ignitor circuit of V_3. The hydrogen thyratron, V_2, is in turn fired by a pulse from the blocking oscillator circuit shown in Fig. 6. The capacitors C_2 and C_{30} are used to isolate the dc level of the blocking oscillator from the dc level of the ignitor circuit of V_3 while allowing the firing signal to be transmitted. The blocking oscillator pulse is initiated by a signal, received at terminal A in Fig. 3, from the sequence control circuits.

The capacitor bank and the trigger capacitors are charged by equipment in the bank charging circuit shown in Fig. 7. The capacitor bank is charged by the three-phase full wave bridge power supply which furnishes a variable output voltage from 0 to over 6000 volts by means of

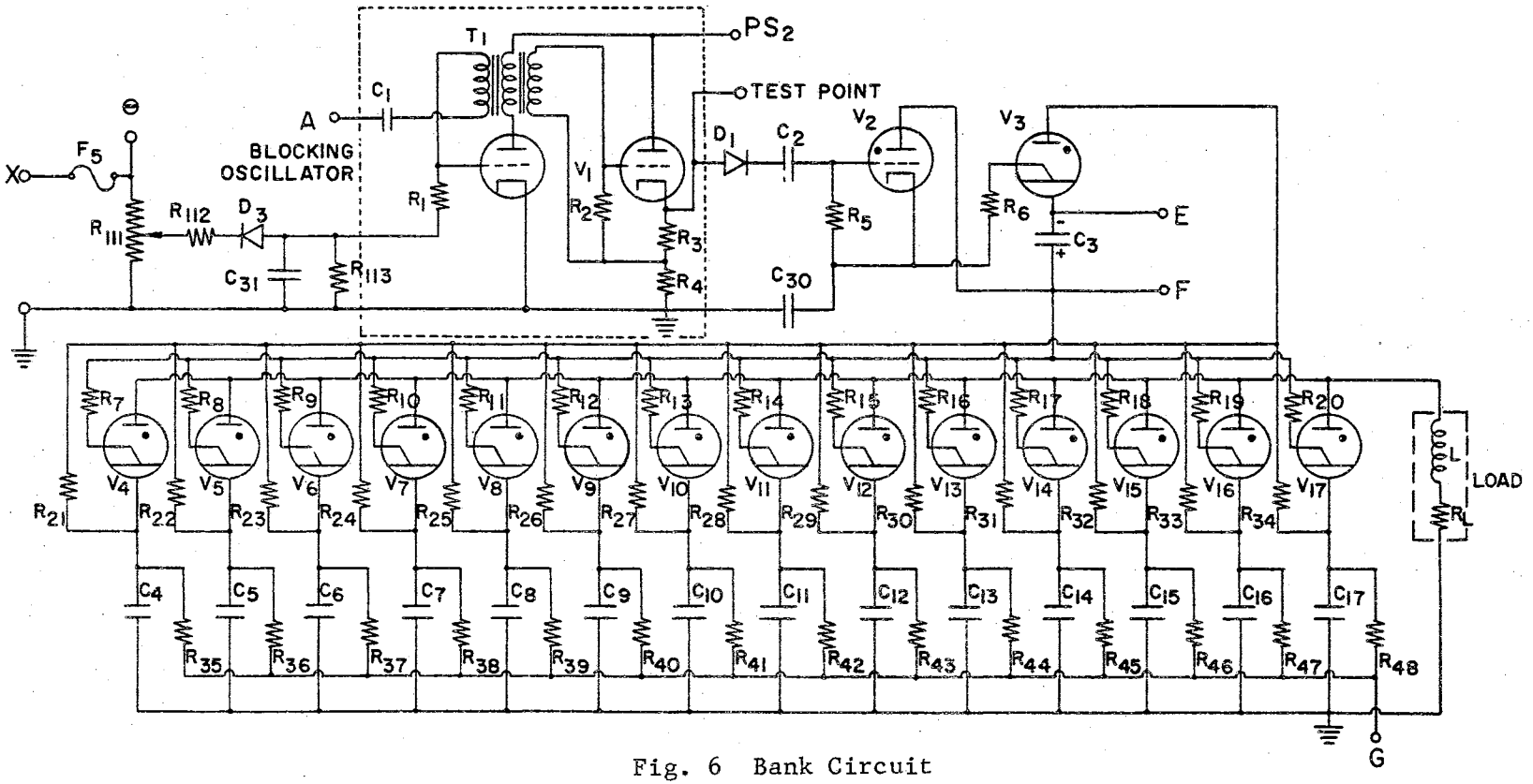

Fig. 6 Bank Circuit

the three-phase variable autotransformer, T_3, in the primary circuit of the high voltage transformer, T_4. The operation of the power supply is controlled by contactor K_1 which operates when it receives a signal from the sequence control circuit. The power supply is capable of charging the capacitor bank to full rated potential in 18 seconds, thus decreasing the time the bank is charged, and allowing rapid repetition of experiments. The trigger capacitors, C_3 and C_{28}, are charged by the two single phase full wave bridge power supplies to a voltage of 1500 to 3000 volts, depending on the setting of the variable autotransformer, T_5. The operation of these power supplies is controlled by a relay, K_4, activated by a signal received from the sequence control circuit. Also shown in Fig. 7 are two Schmitt trigger circuits. One of the circuits is used to furnish a signal to the sequence control circuit when a desired potential is reached. The signal appears at I in Fig. 7 and is due to the operation of relay K_2. The desired voltage level is preset before the bank is charged, by potentiometer R_{51}, and switch S_1. The other Schmitt trigger circuit is set by R_{57} to furnish a signal to the sequence control circuit at J in Fig. 7 when the bank potential reaches 6000 volts and is used as protection against overcharging. Either one of these two signals causes the sequence control circuit to open relay K_1 thus stopping the charging of the bank.

The ignitron tubes, V_4 through V_{17}, used for discharging the capacitor bank into the load lose their rectifying properties for the currents and pulse times used and thus become closed switches conducting equally well in both forward and reverse directions. As stated previously, the crowbar circuit, shown in Fig. 8, stops the current through the magnet after approximately one-half cycle. The crowbar circuit, as used in this

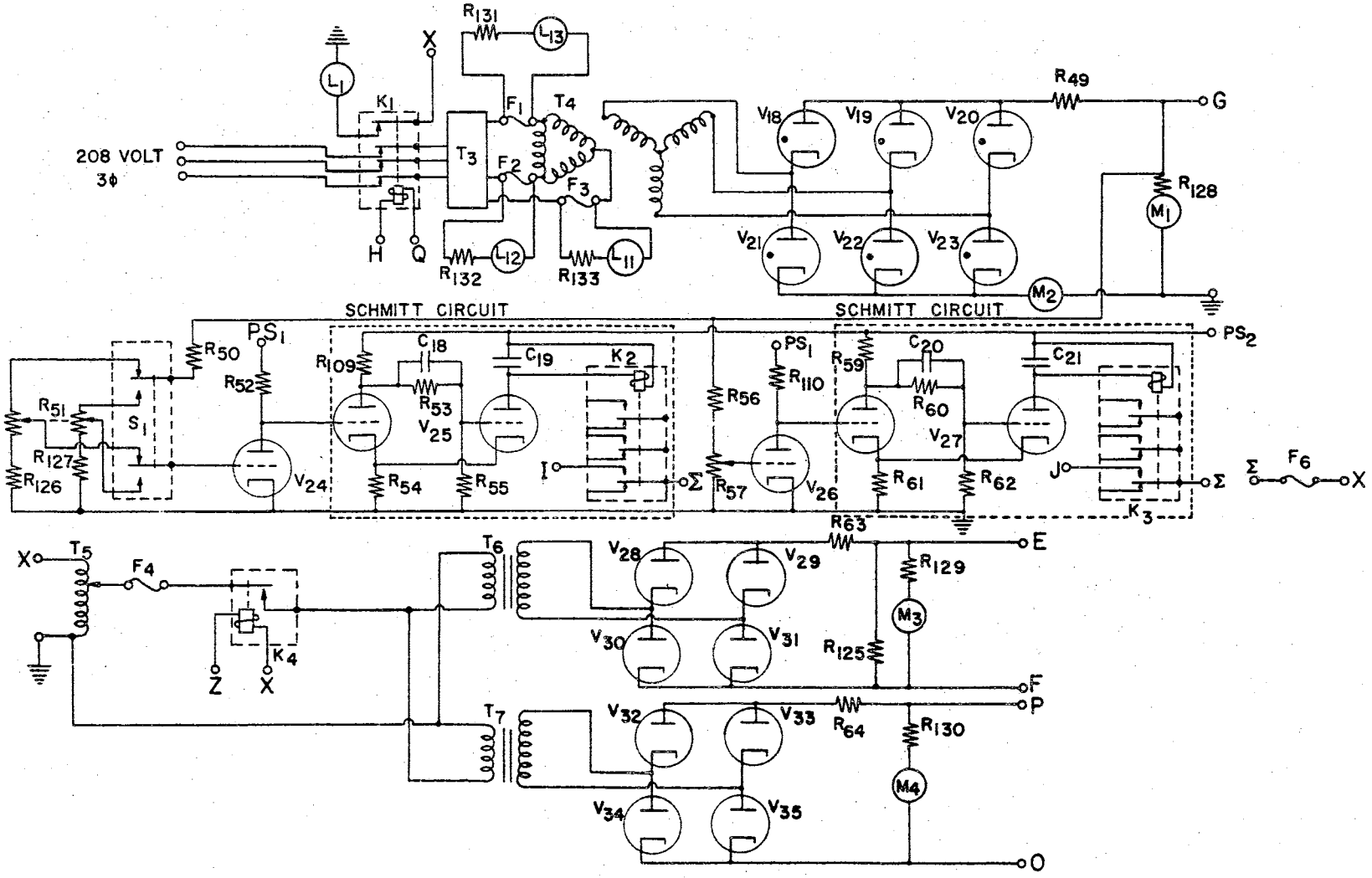

Fig. 7 Bank Charging and Voltage Sensing Circuit

application, protects the electromagnet by providing an essentially resistive, low impedance current path in parallel with the electromagnet after approximately one-half cycle of magnetic field oscillation has taken place. Referring to Fig. 6 and Fig. 8, the crowbar circuit shorts the bank through crowbar resistors R_{35} through R_{48}, and R_{92} through R_{99} by means of ignitron tubes V_{42} through V_{49}. The ignitrons are fired simultaneously by discharge of a trigger capacitor, C_{28}, through their ignitors in the same manner as used for firing the main discharge ignitrons, V_4 through V_{17}. Initiation of the crowbar action takes place after a time determined by the setting of a phantastron delay circuit. The signal which fires the main discharge ignitrons is received at W, Fig. 8, the input to the phantastron delay circuit, when the crowbar circuit is operative. The output of the phantastron delay circuit is a negative gate of length equal to the desired time delay. The delay is variable and its length is adjusted using potentiometer R_{66}. The negative gate is put into a differentiating and pulse forming network whose output is a proper input signal for the blocking oscillator circuit. This signal then fires the blocking oscillator and the crowbar ignitrons, V_{42} through V_{49}, in the same manner that the main discharge ignitrons are fired. As has been shown, the crowbar ignitrons fire after the main discharge ignitrons at a time determined by the phantastron delay circuit. To determine a desirable delay for the crowbar circuit a low voltage (low energy) discharge is made through the electromagnet without the crowbar action. The length of time from the beginning of the discharge to point A, Fig. 5a, is determined and the crowbar circuit is set to operate at the point A to give the desired action.

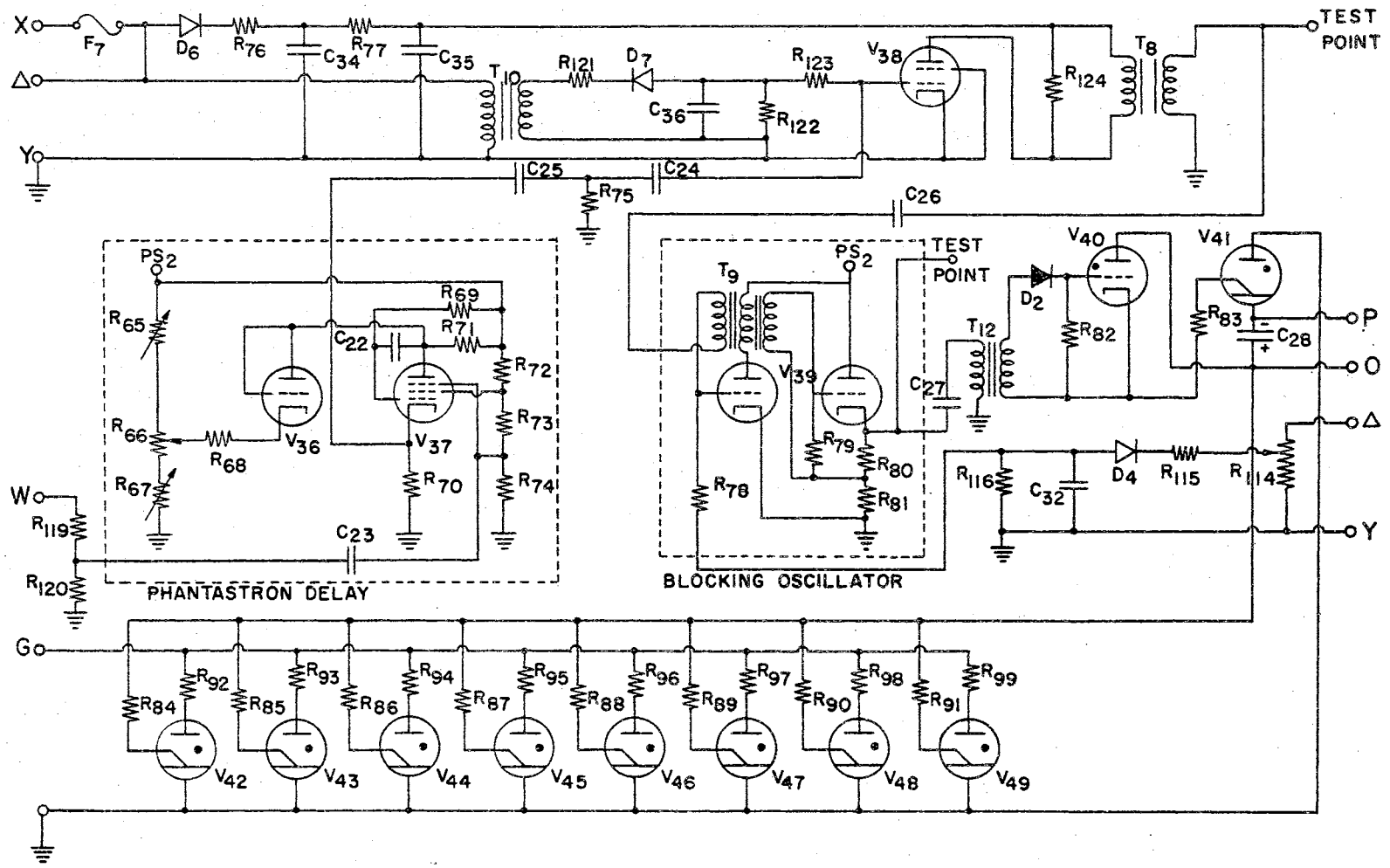

Fig. 8 Crowbar Circuit

The operation of the capacitor bank is controlled by the sequence control circuit, Fig. 9. Terminals H and Q are connected to the operating coil of the relay, K_1, which furnishes power to the charging equipment. Therefore, the operation of the capacitor bank charging circuit is controlled by relays K_5, K_6 and K_7, and switch S_2. Relays, K_6 and K_7, are connected to the Schmitt trigger circuits, Fig. 7, and shut off power to the charging equipment when the desired voltage or an overvoltage is present on the bank. Relay K_5 is connected so as to be self-energizing when the charge start pushbutton, S_7, is pressed. Switch S_2 is a charge halting switch which, when operated, cuts power to the charging circuits and discharges the capacitor bank through resistor R_{104} and the trigger capacitors through resistors R_{100} and R_{102}. These resistors are used to 1) furnish an alternative means of discharging the bank, 2) bleed off the remaining bank energy after a normal discharge (uncrowbarred or crowbarred discharge through the load). Two different modes of operation of the capacitor bank may be selected by means of switch S_8. The circuit diagram, Fig. 9, shows switch S_8 in position for the automatic mode of operation. In this mode, after the desired capacitor bank potential has been set on R_{51} and S_1, Fig. 7, switch S_7 may be operated, thus causing the capacitor bank to be charged to the preset potential and then to discharge automatically through the load. The alternate position of switch S_8 selects the manual mode of operation. With switch S_8 in this position when switch S_7 is pressed, the capacitor bank is charged to the preset potential. Then the power to the capacitor bank charging circuit is cut off, indicator light L_3 comes on indicating the bank is charged, and power is supplied to the three minute time delay relay K_{13}. At any time within the next three minutes switch S_9 may be pressed, thus discharging

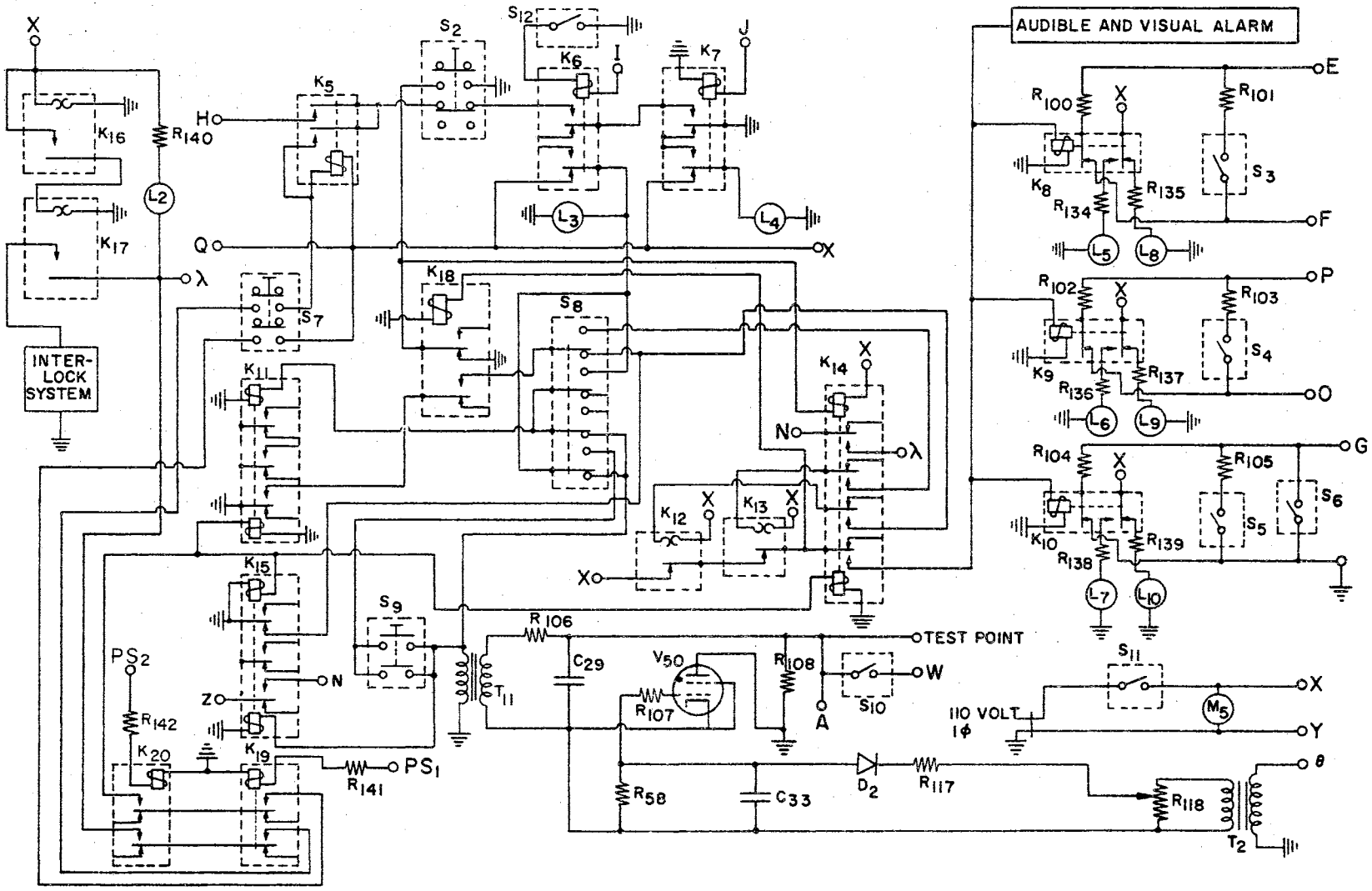

Fig. 9 Sequence Control Circuits

the bank. If the bank is not discharged at the end of the three minute period, the time delay relay, K_{13}, automatically discharges the capacitor bank through resistor R_{104} and the trigger capacitors through resistors R_{100} and R_{102}. After a normal discharge through the load the time delay relay, K_{12}, closes the relays K_8, K_9 and K_{10}, thus completely discharging the bank through the resistors R_{100}, R_{102} and R_{104} (this is necessary since the ignitrons will cease conduction before the capacitor bank is fully discharged). For safety a second set of resistors, R_{101}, R_{103} and R_{105}, is included through which the capacitor bank and trigger capacitors may be discharged by manually operating switches S_3, S_4 and S_5. The switch S_{12} may be used to manually stop the charging of the bank without discharging it. The pulse needed to initiate the action of the blocking oscillator in Fig. 6 (to discharge the bank through the load), and the phantastron delay circuit in Fig. 8 is obtained by furnishing power to the input of transformer T_{11}. Capacitor C_{29} is then charged until the breakdown voltage of tube V_{50} is reached at which point the capacitor, C_{29}, is discharged through resistor R_{108}, thus producing the desired signal pulse. The switch S_{10} is used to make connection to the crowbar circuit.

Table I is a list of the components used in the Pulsed Magnet System.

The capacitor bank is enclosed in a cement block room for safety. Electrical connections are made to a collector plate located outside the room but connected to the capacitor bank by RG-19 coaxial cables, one cable connecting to each capacitor in the bank. Ear protection is worn during the operation of the capacitor bank in case there is a failure of the magnet or collector plate insulation.

TABLE I

PULSED MAGNET SYSTEM COMPONENTS LIST

RESISTORS & POTENTIOMETERS		
R_1	20k	1w
R_2	2.7k	½w
R_3	300	½w
R_4	820	1w
R_5	20k	1w
R_6	12	2w
R_7 to R_{20}	5.6	2w
R_{21} to R_{34}	6.2	2w
R_{35} to R_{48}	.0778	Special Res.
R_{49}	4.17k	2.4kw
R_{50}	5meg	8w
R_{51}	50k,500k Pot(dual)	½w
R_{52}	20k	1w
R_{53}	100k	½w
R_{54}	15k	½w

CAPACITORS		
C_1	.05μf	400VDC
C_2	.01μf	10KVDC
C_3	50μf	3,500VDC
C_4 to C_{17}	180μf	6,000VDC
C_{18}	20μμf	300VDC
C_{19}	0.1μf	400VDC
C_{20}	20μμf	300VDC
C_{21}	0.1μf	400VDC
C_{22}	1,500μμf	300VDC
C_{23}	3,300μμf	500VDC
C_{24}	.05μf	400VDC
C_{25}	500μμf	500VDC
C_{26}	.05μf	400VDC
C_{27}	.1μf	400VDC
C_{28}	20μf	3,500VDC

TABLE I (Continued)

R_{55}	64k	½w	C_{29}	.02μf	200VDC
R_{56}	5meg	8w	C_{30}	.01μf	10KVDC
R_{57}	75k	2w	C_{31},C_{32}	10μf	150VDCW electrolytic
R_{58}	100k	½w	C_{33}	25μf	6VDCW electrolytic
R_{59}	10k	½w	C_{34}	10μf	150VDCW electrolytic
R_{60}	100k	½w	C_{35}	.02μf	200VDCW
R_{61}	15k	½w	C_{36}	25μf	6VDCW electrolytic

SWITCHES

R_{62}	62k	½w	S_1	2PDT	250V	3A
R_{63},R_{64}	25k	100w	S_2	2PDT	110V	10A
R_{65}	10k Pot.	5w	S_3,S_4	1PST Special	3,500V	1A
R_{66}	20k	10-turn linear Pot.	S_5,S_6	1PST Special	6,000V	10A
R_{67}	10k Pot.	5w	S_7	2PDT	110V	10A
R_{68}	22k	½w	S_8	4PDT	110V	3A
R_{69}	1meg	½w	S_9	2PST	110V	½A
R_{70}	3.3k	½w	S_{10}	1PST	250V	3A

TABLE I (Continued)

R_{71}	1meg	½w
R_{72}	47k	½w
R_{73}	22k	½w
R_{74}	2.2k	½w
R_{75}	56k	½w
R_{76}	150	2w
R_{77}	100k	½w
R_{78}	20k	1w
R_{79}	2.7k	½w
R_{80}	300	½w
R_{81}	820	1w
R_{82}	2.5k	1w
R_{83} to R_{91}	12	2w
R_{92} to R_{99}	.0444	Special Res.
R_{100} to R_{103}	25k	100w
R_{104}, R_{105}	1.43k	2.8kw

S_{11}	2PST	110V	25A
S_{12}	1PST	250V	3A

TUBES	
V_1	6SN7
V_2	6268
V_3 to V_{17}	G1-7703
V_{18} to V_{23}	G1-872A
V_{24}	6AS7-GA
V_{25}	5965
V_{26}	6AS7-GA
V_{27}	5965
V_{28} to V_{35}	8020
V_{36}	5814
V_{37}	5725
V_{38}	5727
V_{39}	6SN7

TABLE I (Continued)

R_{106}	100k	½w	V_{40}	6268
R_{107}	100k	½w	V_{41} to V_{49}	G1-7703
R_{108}	51	1w	V_{50}	5727
R_{109}	10k	½w		
R_{110}	20k	1w		
R_{111}	10k Pot.	5w		
R_{112}	150	2w		
R_{113}	100k	½w		
R_{114}	10k Pot.	5w		
R_{115}	150	2w		

TRANSFORMERS

T_1	300V	1-1-1	pulse
T_2	115V to 2.5V		
T_3	240V	3 phase	9.7KVA variable auto-transformer
T_4	3-5KVA, 4,800-120/240V transformers connected for 3 phase operation		
T_5	120V	2.3KVA	variable auto-transformer
T_6	115V to 3000V at 350ma.		10KV insulation

TABLE I (Continued)

R_{116}	100k	½w	T_7	120V to 1,900V		.7KVA
R_{117}	10	1w	T_8, T_9	300V	1-1-1	pulse
R_{118}	10k Pot.	5w	T_{10}	115V to 2.5V		
R_{119}	1500	½w	T_{11}	115V	35VA	isolation
R_{120}	510	½w	T_{12}	2000V	1-2-1	pulse
R_{121}	10	1w	METERS		DIODES	
R_{122}	1.5k	½w	M_1	0-7,500 VDC	D_1, D_2	3,000 PIV, 750 ma.
R_{123}	100k	½w	M_2	0-3.0 ADC	D_3 to D_7	200 PIV 750 ma.
R_{124}	51	½w	M_3, M_4	0-5,000 VDC		
R_{125}	350k	75w	M_5	0-99,999.9 hrs.		
R_{126}	75k	½w	PANEL LIGHTS			
R_{127}	30k	1w	L_1	Red Jewel	1"	
R_{128}	7.5meg	15w	L_2	Red Jewel	½"	

TABLE I (Continued)

R_{129}, R_{130}	5meg	10w
R_{131} to R_{133}	1k	25w
R_{134} to R_{140}	700	20w
R_{141}	12k	½w
R_{142}	56k	2w

L_3	Green Jewel	1"
L_4	Amber Jewel	1"
L_5 to L_7	Red Indicator	
L_8 to L_{10}	Green Indicator	
L_{11} to L_{13}	Red Indicator	

RELAYS

K_1	3PST	240V	90A
K_2, K_3	3PDT	10k ohm	6.1 ma
K_4, K_5	2PST	110V	10A
K_6, K_7	2PDT	110V	10A
K_8, K_9	1PST and 1PDT	3,500V 110V	1A 1A Special Relay
K_{10}	1PST and 1PDT	6,000V 110V	10A 1A Special Relay
K_{11}	4PDT	110V	10A Latching Relay
K_{12}	1PST-NC	110V	2 sec. time Delay Relay

FUSES

F_1	20 amp. Buss super lag
F_2	20 amp. Buss super lag
F_3	20 amp. Buss super lag
F_4	5 amp. 250 V
F_5	1 amp. 250 V
F_6	1 amp. 250 V
F_7	1 amp. 250 V

POWER SUPPLIES

PS_1	+100 VDC	rated 100 ma. 0.1% regulation
PS_2	+300 VDC	rated 100 ma.

TABLE I (Continued)

K_{13}	1PST-NC	110V	180 sec. time Delay Relay
K_{14}, K_{15}	4PDT	110V	10A Latching Relay
K_{16}, K_{17}	1PST-NC	110V	180 sec. time Delay Relay
K_{18}	2PDT	110V	10A
K_{19}, K_{20}	2PDT	10k ohm 4.5 ma.	

The DC Magnet System

The magnetoresistance effect at low magnetic fields was observed in diamond using a Varian Associates Model V-4004, 4 inch dc electromagnet with 2 inch tapered pole caps to furnish the magnetic field. For the pole separations used the magnet was capable of producing continuously a constant magnetic field of 16,500 gauss. Higher fields could be obtained for short durations. The magnet was water cooled for magnetic fields near its limit. Electrical power for the magnet was obtained from a large capacity rectifier board.

The Sample Mount

Two different types of sample mounts were used in the experiment. Both types were made of polystyrene. The mount shown in Fig. 10 was used for transverse magnetoresistance measurements in the pulsed magnet and for both transverse and longitudinal magnetoresistance measurements in the dc magnet. Figure 11 shows the mount used for longitudinal magnetoresistance measurements in the pulsed magnet. Current leads in both mounts were of #36 B&S gauge magnet wire, and the potential leads were of #40 B&S gauge magnet wire. For pulsed magnetic field magnetoresistance measurements the threaded portions of the sample mounts were screwed into a ½ inch diameter, 6 inch long, lucite rod drilled along the axis to allow passage of the leads. Using this rod the sample was placed at the center of the magnet. For magnetoresistance measurements using the dc magnet the threaded portions of the sample mounts were screwed into a ½ inch diameter copper rod drilled along the axis to allow passage of the leads. The copper rod was surrounded along most of its length by a jacket through which water

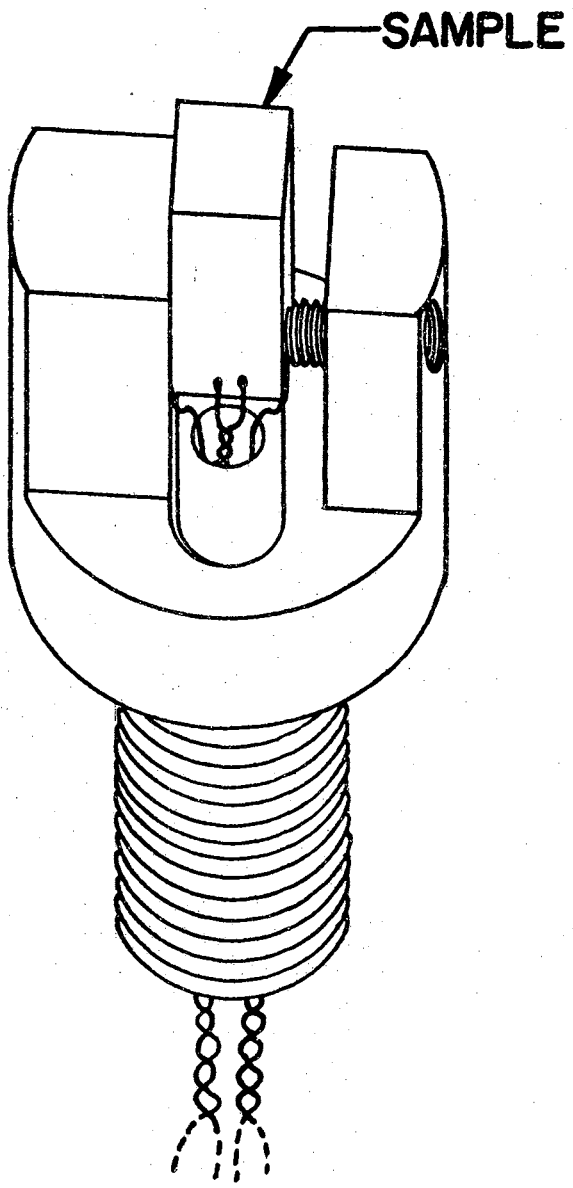

Fig. 10 Transverse Sample Mount

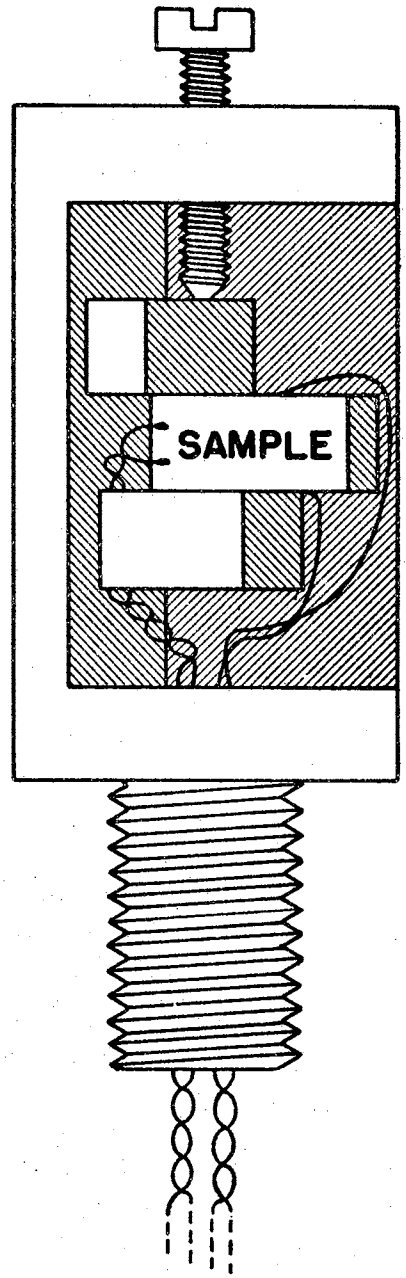

Fig. 11 Longitudinal Sample Mount

from the constant temperature bath flowed. The copper rod and jacket are shown in Fig. 12. The end of the copper rod opposite the sample was threaded to fit a ¼ inch diameter stainless steel rod. This stainless steel rod supported the copper rod, jacket, sample, and sample mount in an insulated cavity between the poles of the dc magnet while offering some resistance to heat conduction out of the cavity. A tubular brass heat shield was fitted around the diamond and the polystyrene sample mount and fastened to the copper rod to provide a more constant temperature for the diamond by shielding it from convection currents. The diamond is then in an inner cavity whose limits are essentially at the temperature of the copper rod which is kept at a constant temperature by water from the constant temperature bath. Contacts to the diamond were made by several different methods. Spring loaded sharpened tungsten points were tried, both on the diamond surface itself and then on silver paint spots on the diamond surface. Indium solder contacts were tested as were silver paint contacts. These contacts in all instances were either much better or were successful where they were not previously if contact was made to an edge of the diamond instead of to a polished surface. Contacts were also put on the diamond by first coating the area to which contact is to be made with a suspension of titanium hydride in amyl acetate, then applying a thin, even layer of an alloy powder over the titanium hydride. The alloy powder is held in place by applying more amyl acetate after the powder is in place. The alloy powder, Incusil 15, size 325 mesh, is a commercial alloy of indium, silver and copper. The diamond is then heated at 780°C for 4 minutes at a pressure of less than 5×10^{-5} mm of Hg. The resulting contacts are mechanically very strong. Electrically they are

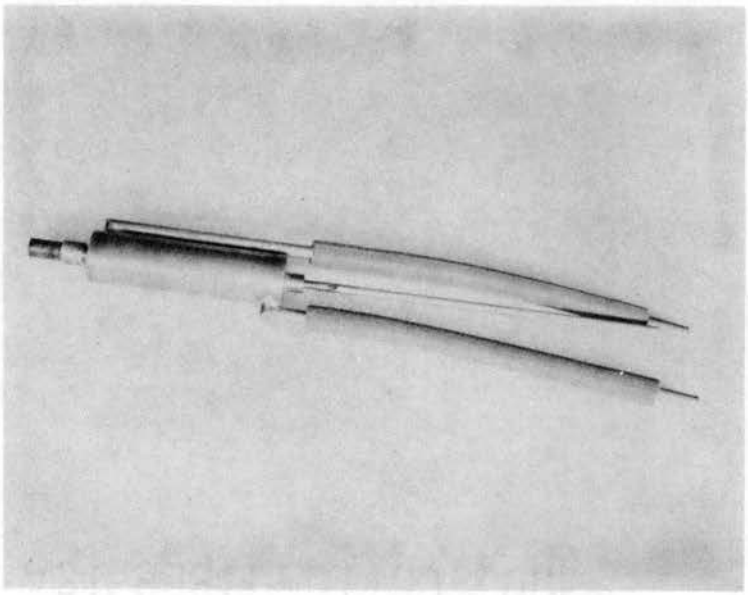

Fig. 12 External Constant Temperature Bath Chamber

much lower resistance and less noisy than any of the previous contacts used. They also have the advantage that they may be used on the polished faces. A disadvantage is that when the contact is removed the surface of the diamond may be slightly eroded. These contacts were used for the bulk of the magnetoresistance measurements. The contact leads were fastened to these contacts with silver paint.

CHAPTER IV

DESCRIPTION OF THE EXPERIMENTS

The Experimental Method

In magnetoresistance studies involving a rectangular parallelepiped, the arrangement of the experiment is usually as shown in Fig. 13. The current contacts cover the ends of the sample in order to provide a uniform current density throughout the sample. The resistor R_1 is a rheostat used to vary the current through the sample. A known value standard resistor, R_2, is used to determine the current through the sample. R_1 is chosen large compared to the resistance of the sample (whether the sample is in or out of the magnetic field). This is done to make the sample current approximately independent of the magnetoresistance effect. In this approximation the change in resistance is given by

$$\Delta R = \frac{\Delta V}{I_o}$$

where I_o is the current through the sample when the magnetic field is zero, and ΔV is the change in the potential difference between the potential probes.

If, as in Fig. 14a, the magnetic field H is directed along the normal to the sample ends bearing the current contacts, the effect is called longitudinal magnetoresistance. If the magnetic field H is directed normal to a line thru the centers of the current contacts, as in Fig. 14b, the effect is called transverse magnetoresistance.

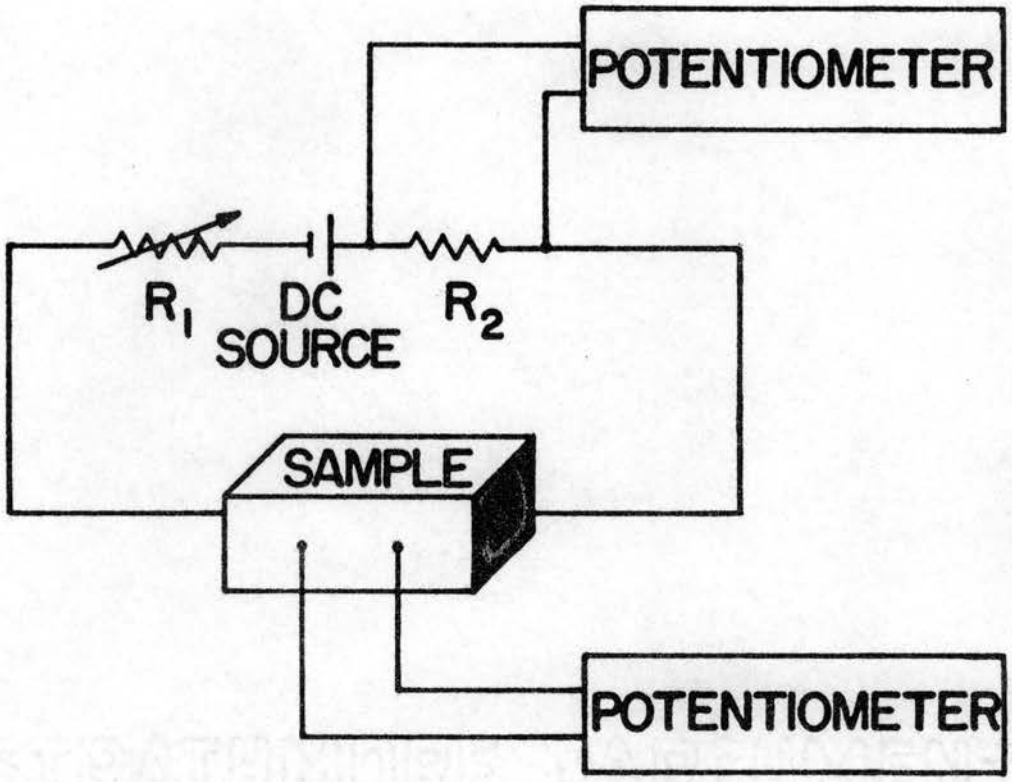

Fig. 13 Magnetoresistance Measuring Circuit

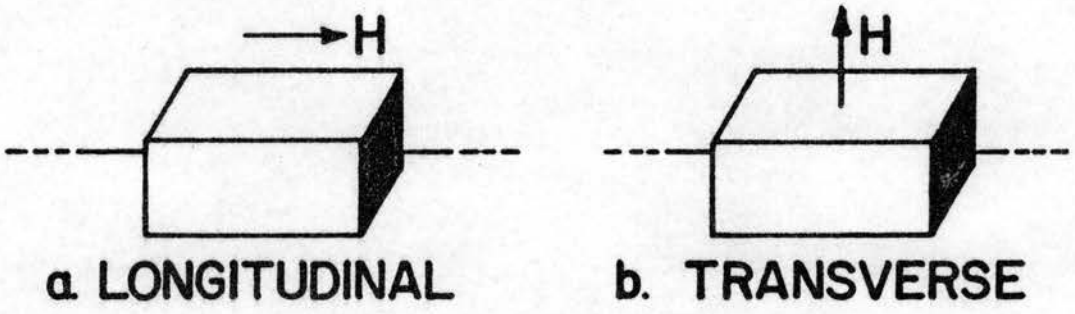

Fig. 14 Longitudinal and Transverse Magnetoresistance

There are several difficulties with the simple theory outlined so far. Any change in the potential difference not caused by magnetoresistance will cause error in the experiment. In particular if the resistance changes during the measurement due to any cause except the magnetic field, of if such a change due to the magnetic field is dependent on the sample geometry there will be an error introduced in the measurement. Also changes in the potential difference not due to a change in resistance will cause an error. The following paragraphs list some of the sources of error in the magnetoresistance experiment.

The resistivity of semiconductors varies markedly with temperature. Therefore the sample being studied must be kept at a constant temperature during the magnetoresistance measurement. This is done by keeping the sample holder in contact with a constant temperature bath. As an added precaution each magnetoresistance measurement can be bracketed by measurements of the sample resistance at zero magnetic field. In addition the current through the sample should be small enough so that Joule heating of the sample is neglible.

Consider the experimental arrangement shown in Fig. 15 for transverse magnetoresistance. Due to the Ettinghausen effect a temperature gradient will appear in the y-direction if an electric current flows in the x-direction and a magnetic field exists in the z-direction. This gradient, ΔT, is given by

$$\Delta T = P\frac{IH}{b}$$

where P is the Ettinghausen coefficient, and H is the magnetic field strength perpendicular to the current I. Due to the Righi-Leduc effect a temperature gradient appears in the y-direction when a thermal current

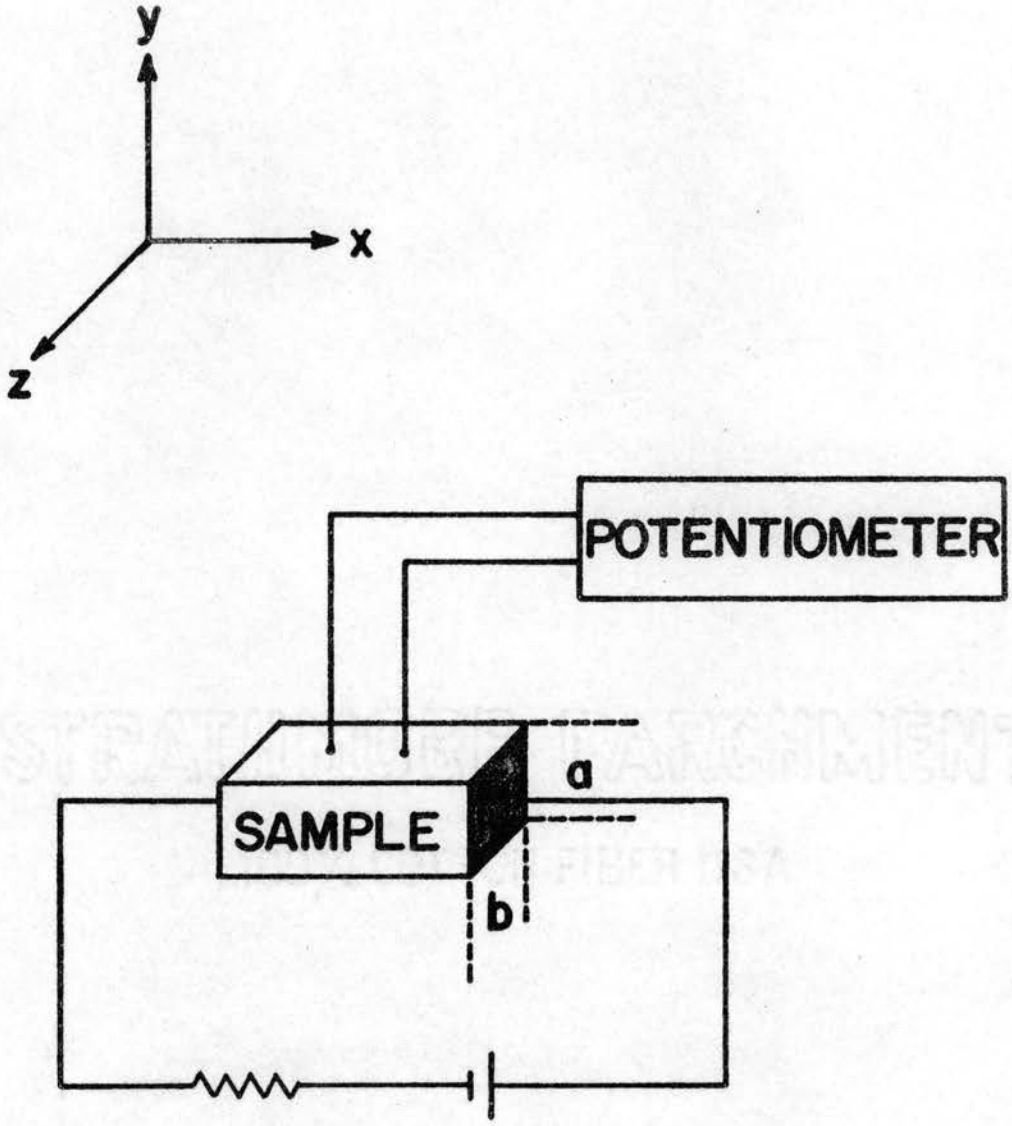

Fig. 15 Illustration of the Thermomagnetic Effects

flows in the x-direction and a magnetic field exists in the z-direction. This gradient is given by

$$\Delta T = S\frac{W_x Ha}{k}$$

where S is the Righi-Leduc coefficient, W_x is the thermal current density, and k is the coefficient of thermal conductivity. Due to the Nernst effect, if there is a thermal current in the y-direction and a magnetic field in the z-direction there exists a potential gradient in the x-direction. This gradient, E_n, is given by

$$E_n = Q\frac{W_y H}{k}$$

where Q is the Nernst coefficient. The Ettinghausen effect directly produces such a thermal current in the y-direction. Since a thermal current exists in the x-direction from the Peltier effect, the Righi-Leduc effect also produces a temperature gradient in the y-direction. Now consider the experimental arrangement shown in Fig. 16 for transverse magnetoresistance. Since the current and magnetic field have the orientation shown in Fig. 16, there will be an electric field, the Hall field, perpendicular to J and H, due to the Hall effect and thus a potential gradient will be set up between the upper and lower faces of the sample. If then the sample potential probes are not located on the same Hall equipotential line there will be a potential across the probes due to the Hall effect.

Unfortunately, it is impossible to directly separate all of these effects from the magnetoresistance effect. This may be seen by considering whether the potentials for the various effects are odd or even in the

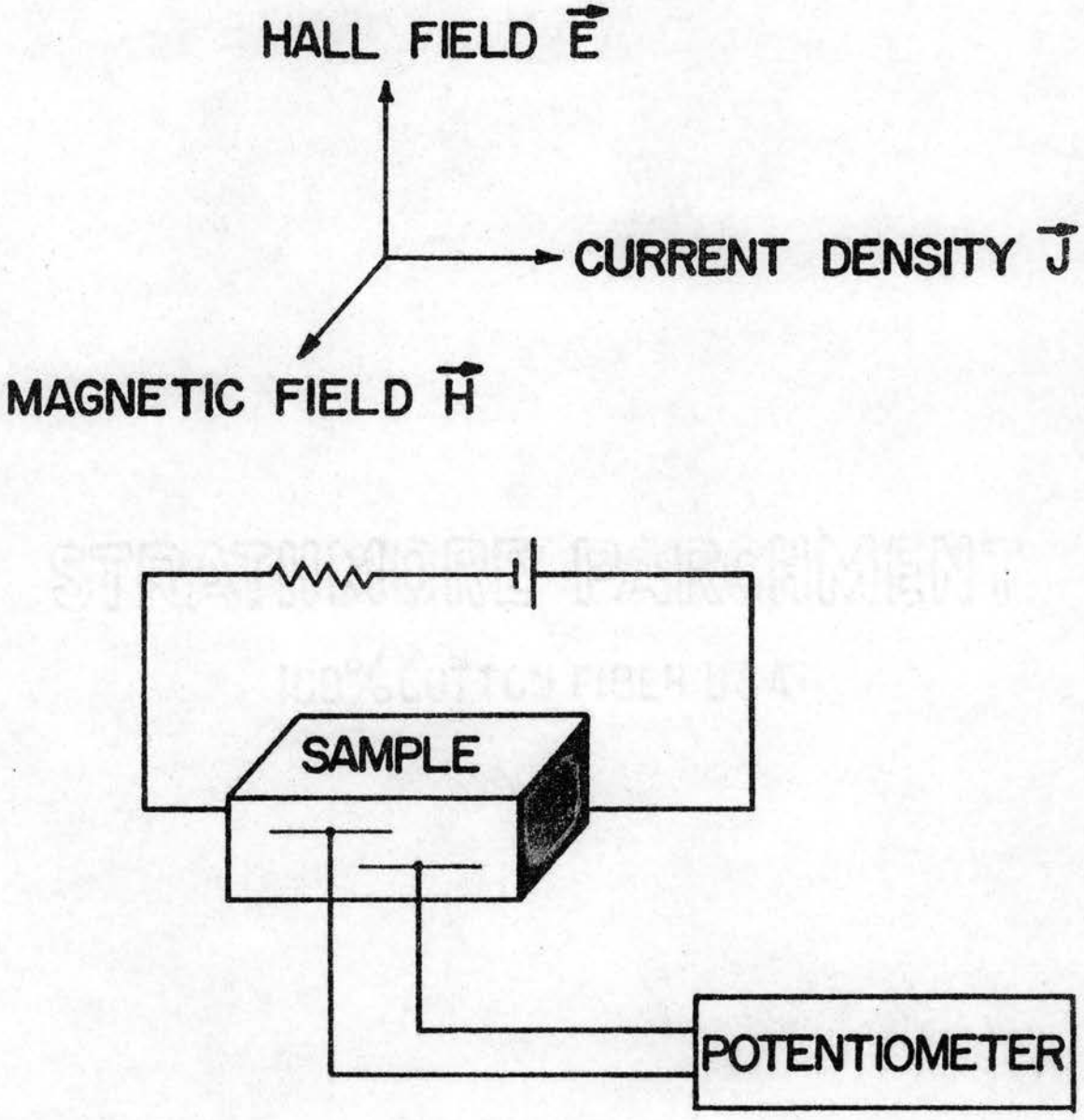

Fig. 16 Source of Error Due to the Hall Effect

magnetic field, H, and the sample current, I. The potential due to the magnetoresistance effect is odd in I and even in H. The Ettinghausen effect, which produces a temperature gradient in the y-direction, is odd in I. Also, if, in the Righi-Leduc effect, the thermal current in the x-direction is produced by an effect odd in I, such as the Peltier effect, then the Righi-Leduc effect is odd in I. Now since the temperature gradients in the y-direction produced by the Ettinghausen and Righi-Leduc effects are odd in H, and the Nernst effect is odd in both the thermal current density and H, the potential produced by the Ettinghausen and Righi-Leduc effects through the Nernst effect is even in H (if the magnetic field is reversed the temperature gradients produced by the Ettinghausen and Righi-Leduc effects are reversed, thus reversing their contribution to the thermal current density, W_y, but H is also reversed in the expression for the Nernst potential so there is no change in sign of the potential). Thus the above potentials are odd in I and even in H. If there is a thermal gradient in the y-direction due to some effect even in H then the resulting part of the Nernst potential will be odd in H and either even or odd in I. The potential caused by the probes being on different Hall equipotential lines is odd in I and odd in H. To shorten the discussion let us define V_{OIEH} to be the potential due to effects odd in I and even in H, V_{OIOH} to be the potential due to effects odd in I and H, and define V_{EIOH} and V_{EIEH} similarly. For a particular I and H let a measurement V_1 be taken. Then

$$V_1 = V_{OIEH} + V_{OIOH} + V_{EIEH} + V_{EIOH}.$$

Reverse the current and then measure the potential

$$V_2 = - V_{OIEH} - V_{OIOH} + V_{EIEH} + V_{EIOH}.$$

Now with the current again in the forward direction reverse the magnetic field, then measure the potential

$$V_3 = V_{OIEH} - V_{OIOH} + V_{EIEH} - V_{EIOH}.$$

Now again reverse the current and measure the potential

$$V_4 = - V_{OIEH} + V_{OIOH} + V_{EIEH} - V_{EIOH}.$$

From the above equations we can write

$$\frac{V_1 - V_2}{2} = V_{OIEH} + V_{OIOH}; \quad \frac{V_3 - V_4}{2} = V_{OIEH} - V_{OIOH}.$$

Now combining these equations we obtain

$$V_{OIEH} = \tfrac{1}{4}[V_1 - V_2 + V_3 - V_4].$$

Thus all effects not odd in I and even in H can be separated from V_{OIEH} by this method. However the previously mentioned Ettinghausen and Righi-Leduc (in conjunction with the Peltier effect) effects give rise to a potential odd in I and even in H. V_{OIEH} then contains these potentials as well as the potential due to the magnetoresistance effect.

Consider the case for longitudinal magnetoresistance where the experimental arrangement is as shown in Fig. 17. There is no Ettinghausen temperature gradient produced in the y-direction, except as a secondary effect, since the current I does not flow in the x-direction. If there is a thermal current in the x-direction there could be a Righi-Leduc temperature gradient in the y-direction. Also if for any other reason there is a thermal gradient set up in the y-direction there will be a

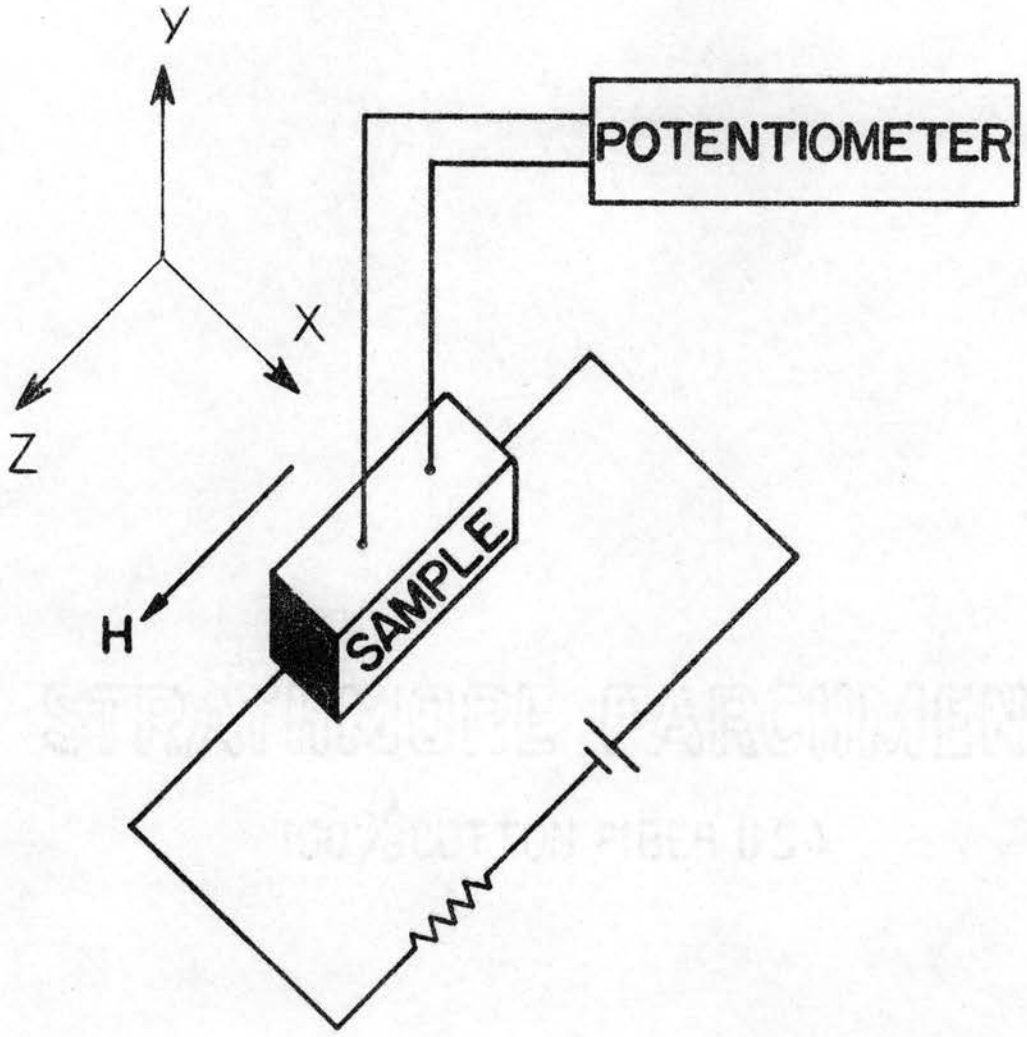

Fig. 17 Error in the Longitudinal Case

potential gradient in the x-direction due to the Nernst effect. If the probes are misaligned they may lie on two different equipotentials of this gradient. This source of error is easily prevented by positioning the probes on the face normal to the x-direction. However the previously described method of cancelling unwanted effects should be used to insure that only effects odd in I and even in H are recorded.

The Experiment Using the Pulsed Magnet System

Figure 18 shows a block diagram of the measuring circuit. The sample, mounted on the sample mount, was inserted in the electromagnet. The potential probes were connected to the input of a Tektronix Type L plug-in unit used in a Tektronix Type 551 Dual Trace Oscilloscope. The sweep was triggered at the start of the discharge by bringing the magnet voltage in on the other beam of the oscilloscope through a Tektronix Type K plug-in. A high voltage probe with 1000-1 attenuation was used to make connection to the high magnet voltage. The magnet and sample were surrounded by an asbestos paper enclosure closed at two ends by cotton to form a constant temperature chamber and permit exit of leads. The chamber was heated to the desired sample temperature by passing current through a length of nichrome wire which was wrapped around the magnet. The temperature in the chamber was measured by means of a iron-constantan thermocouple and a potentiometer. The potential across the potential probes for no magnetic field was measured by the Leeds and Northrup Type K-3 potentiometer. Resistor R was chosen large enough so that the change in current caused by the magnetoresistance effect was less than one per cent of the current. The capacitor bank was charged to the desired potential level and discharged through the magnet

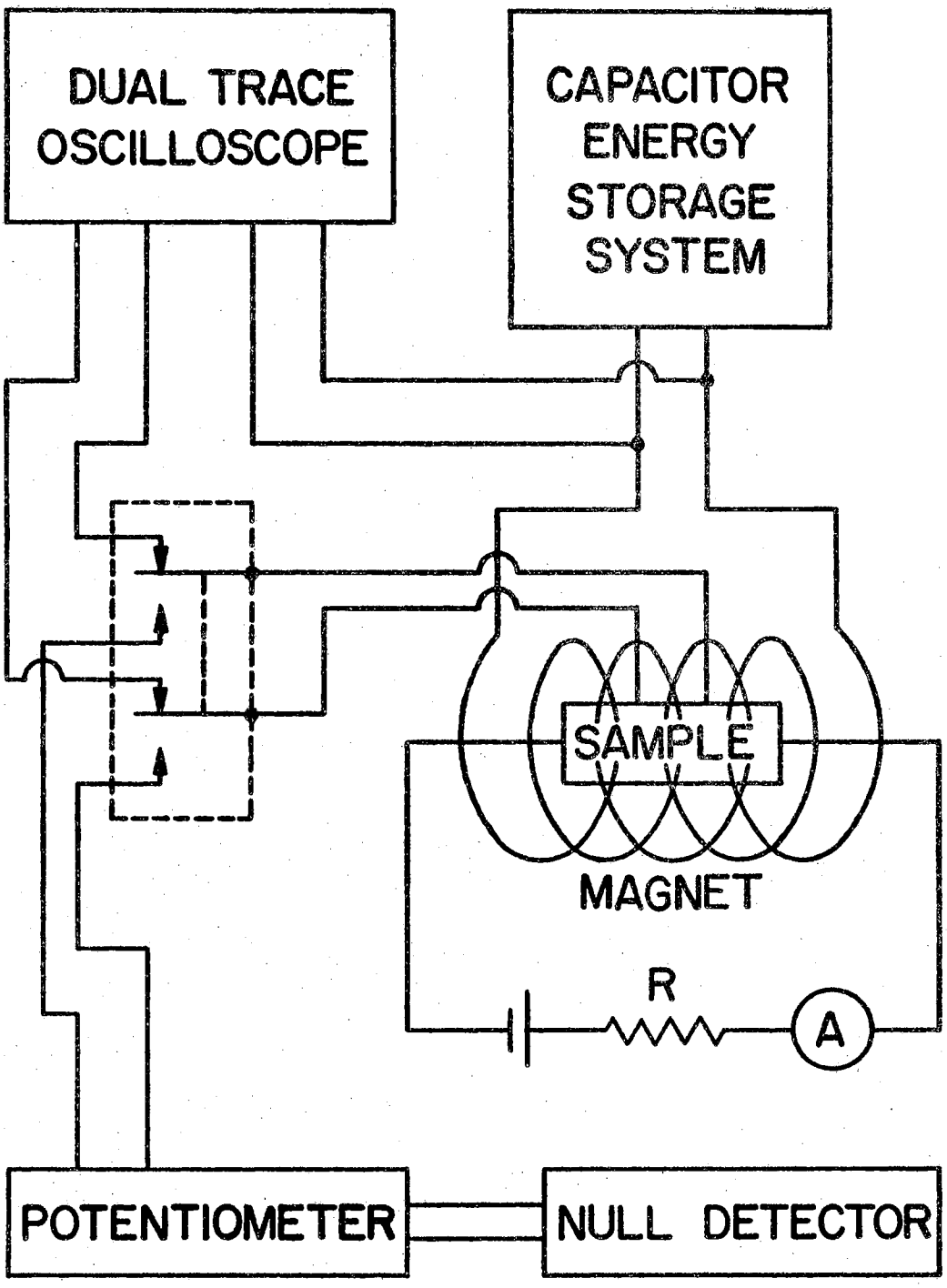

Fig. 18 Measuring Circuit for Pulsed Magnetic Fields

(Another discharge with the capacitor bank at the same potential level but with a search coil in the position of the sample is used to measure the magnetic field. The output of the search coil is integrated by a Tektronix Type O plug-in unit used in the Tektronix Type 551 Dual Trace oscilloscope.). The resulting trace was due to the sum of a potential due to the magnetoresistance effect, potentials due to the Hall and thermomagnetic effects discussed earlier, a potential due to pickup by the potential probes being located in the varying magnetic field, and, in the case where the potential contact resistance was high (contacts on the (110) face on the blue end), a potential due to pickup that was independent of the sample current and the magnetic field direction at the sample. In the case where the potential due to the last type of pickup (that which was independent of the magnetic field direction at the sample) was absent, four measurements were taken, one for each possible combination of sample current direction and magnetic field direction, and the results combined as described in The Experimental Method, page 42, to get the desired potential. In the case where the potential due to the pickup which was independent of magnetic field direction in the sample was present, for each of the four combinations of direction of the sample current and magnetic field, another discharge was made with no current through the sample to isolate the pickup. The potential used in the analysis given on page 42 was then the difference between the trace recorded with sample current on and the trace recorded with no sample current. The traces were recorded on film using a Hewlett-Packard Model 196A oscilloscope camera.

The Experiment Using the DC Magnet

The magnetoresistance effect at low magnetic fields was observed in diamond using a Varian Associates Model V-4004 four inch electromagnet to furnish the magnetic field. Figure 19 shows a block diagram of the measuring circuit. The potentiometer, a Leeds and Northrup Type K-3 Universal Potentiometer using a Leeds and Northrup Cat. 9834 DC Null Detector, was used to measure the change in potential caused by the magnetic field. The resistor R was chosen large enough so that the change in current caused by the magnetoresistance effect was less than one per cent of the current. The current through the sample was measured potentiometrically by measuring the voltage drop across the 1000 ohm resistor. The sample was kept at a desired temperature by being in contact with a holder through which water from a constant temperature bath circulated. The temperature controller used in the bath was a Bayley Instrument Company Model 117 Precision Temperature Controller. For the particular pole separation used a plot was made of the magnetic field versus the current through the magnet. An F. W. Bell Model 300 gaussmeter was used to make the measurement of the magnetic field. Then by setting the current through the magnet correctly, any desired magnetic field was reset with great precision. The magnetic field due to the pole pieces with no magnet current was never larger than 170 gauss. As was explained in an earlier section, four potentials were measured for a particular magnetic field strength and sample orientation, one for each possible combination of magnetic field direction and sample current direction. The desired potential was then found from these four measurements.

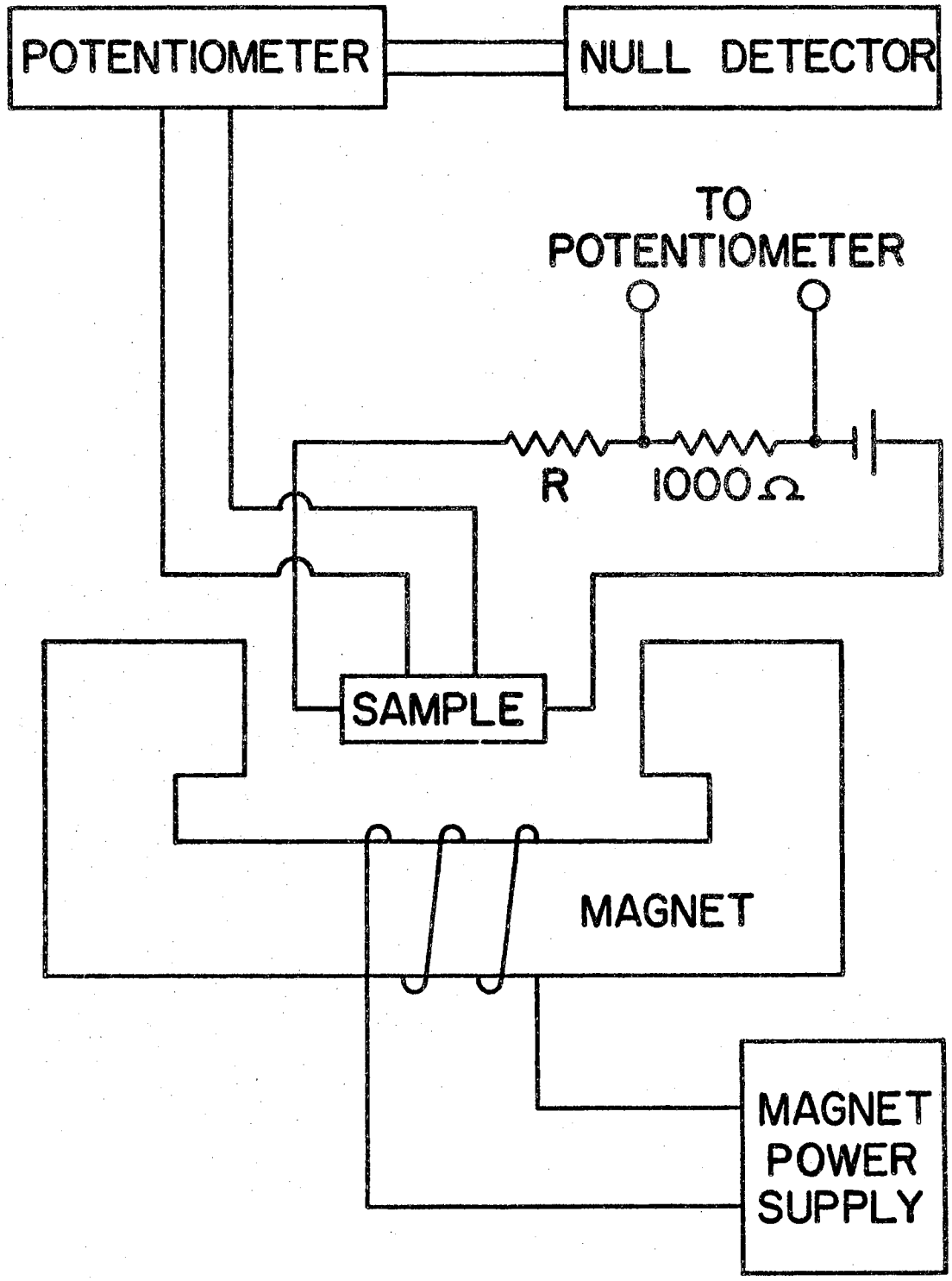

Fig. 19 Measuring Circuit for DC Magnetic Fields

CHAPTER V

RESULTS

The Specimen

The specimen examined in this study was a semiconducting diamond geometrically close to a rectangular parallelopiped with sides equal to the dimensions listed in Fig. 20. The large faces lie fairly close to (111) planes (about 8° off). The faces with dimensions 6.5 millimeters by 2.5 millimeters are close to (113) planes (within 2°). The small faces are close to (110) planes (within $\frac{1}{2}^{\circ}$). The faces are highly polished for optical work. The diamond can be classified visually into a blue region and a clear region, as illustrated in Fig. 20. The blue region extends from one end to about 2 millimeters into the diamond. The color, though faint, is easily visible to the unaided eye. The two regions, though both semiconducting, show remarkable differences. In the blue end the resistivity ranges from 62.5 ohm-cm to 287 ohm-cm, while in the clear end it varies from 177,000 ohm-cm to 350,000 ohm-cm (23, 24). Much experimental work has been done on this diamond (23, 24). This diamond is referred to as DS-2 in the final report by Leivo et. al. (24).

Magnetoresistance as a Function of Angle Between the Current and the Magnetic Field

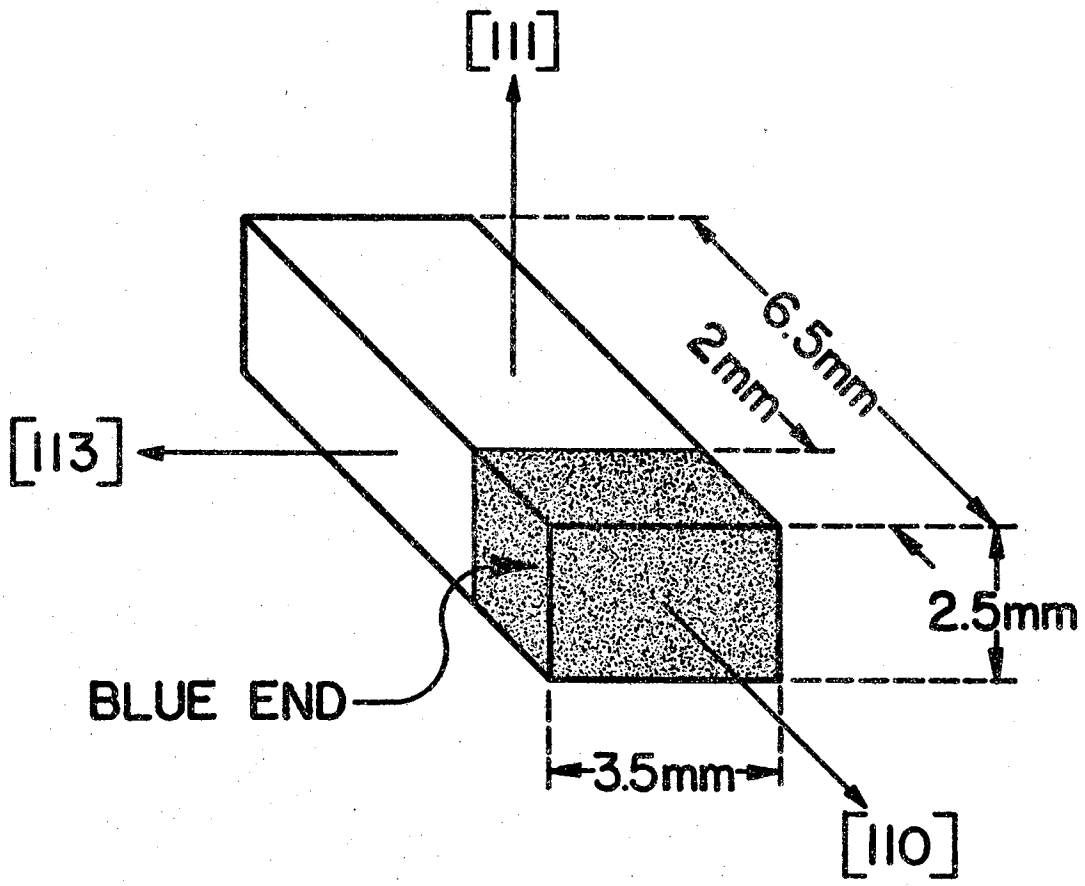

Fig. 20 The Specimen

In this measurement the dc magnet was used to provide a constant magnetic field of 4050 gauss. The measuring apparatus used was described earlier in Chapter IV. A graduated circle was used to determine the orientation of the diamond with the magnetic field. The current contacts were applied to the (113) faces. Magnetoresistance as a function of the angle, Θ, between the current and the magnetic field was measured for Θ varying in increments of 15° between 0° and 360°. Rotation of the diamond was about an axis perpendicular to the (111) face of the diamond. The measurement was performed at a sample temperature of $307.7^{\circ}K$. Figure 21 is a graph of the data obtained in this experiment. The data can be compared with that of Mitchell and Wedepohl (13) who show similar results with their diamond; however, the present results seem to be more regular. This is probably due to the use of the titanium hydride contacts described earlier.

Longitudinal Magnetoresistance

Longitudinal magnetoresistance effects were investigated using both the dc magnet and the pulsed magnet system as described in Chapter IV with the exception that a different oscilloscope (a single beam Tektronix Type 503) was used in making the measurements in the [113] direction with pulsed magnetic fields. Longitudinal magnetoresistance was obtained in the [113] direction (current contacts on the (113) face) and in the [111] (current contacts on the (111) face). The sample was at a temperature of $307.7^{\circ}K$ during the measurements. The measurement in the [113] direction was slightly more reliable because of the lower resistance of the potential probe contacts used for that direction.

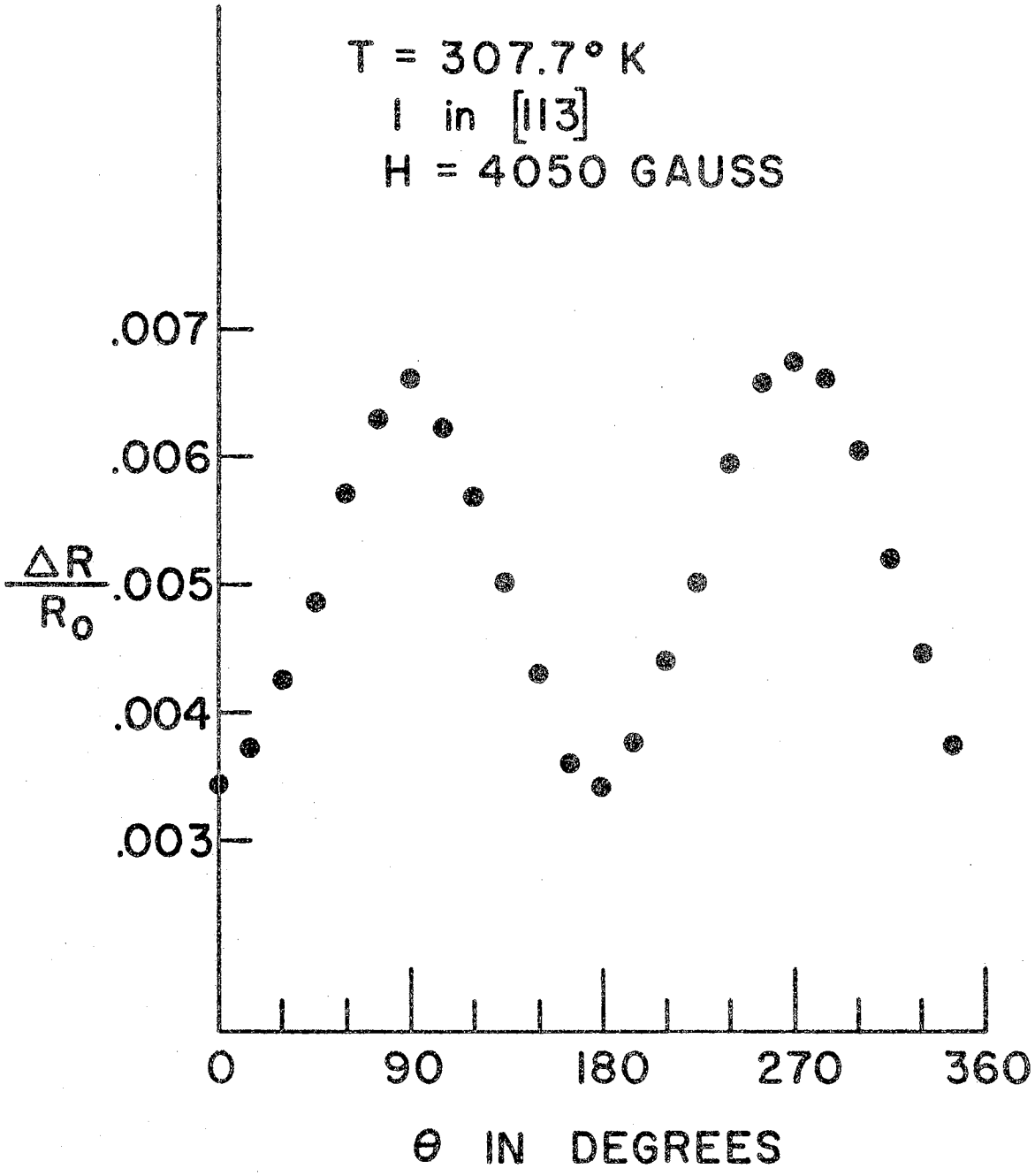

Fig. 21 Magnetoresistance as a Function of Angle θ

Figure 22 is a graph of the longitudinal magnetoresistance in the [113] direction for low magnetic fields. The experimental points represented by dots were obtained using the dc magnet, and the points represented by circles were obtained from data taken with the pulsed magnet using a maximum field of about 47.5 kilogauss. The agreement between the measured magnetoresistance for pulsed and dc magnetic fields is seen to be good.

A graph of the longitudinal magnetoresistance in the [111] direction for low magnetic fields is shown in Fig. 23. The experimental points represented by circles were obtained using the pulsed magnet at a maximum field of about 46.5 kilogauss. The data obtained using the pulsed magnet is seen to agree fairly closely with that obtained using the dc magnet.

Longitudinal magnetoresistance in the [113] direction is shown in Fig. 24 for both low and high magnetic fields. In these measurements the magnetic field was furnished by the pulsed magnet system. In studying the longitudinal magnetoresistance in the [113] direction magnetoresistance versus magnetic field data was measured using four different peak magnetic fields, and points from the four resulting sets of magnetoresistance versus magnetic field data were used in Fig. 24. The four peak magnetic fields used were 23.6 kilogauss, 47.6 kilogauss, 97.5 kilogauss and 166.8 kilogauss. Thus the data on longitudinal magnetoresistance is seen to be reproducible and to extend smoothly to high magnetic fields. The highest magnetic field used was 166.8 kilogauss. All measurements of magnetoresistance in pulsed magnetic fields were taken using the wire wound magnet described earlier. An attempt was made to use the helical

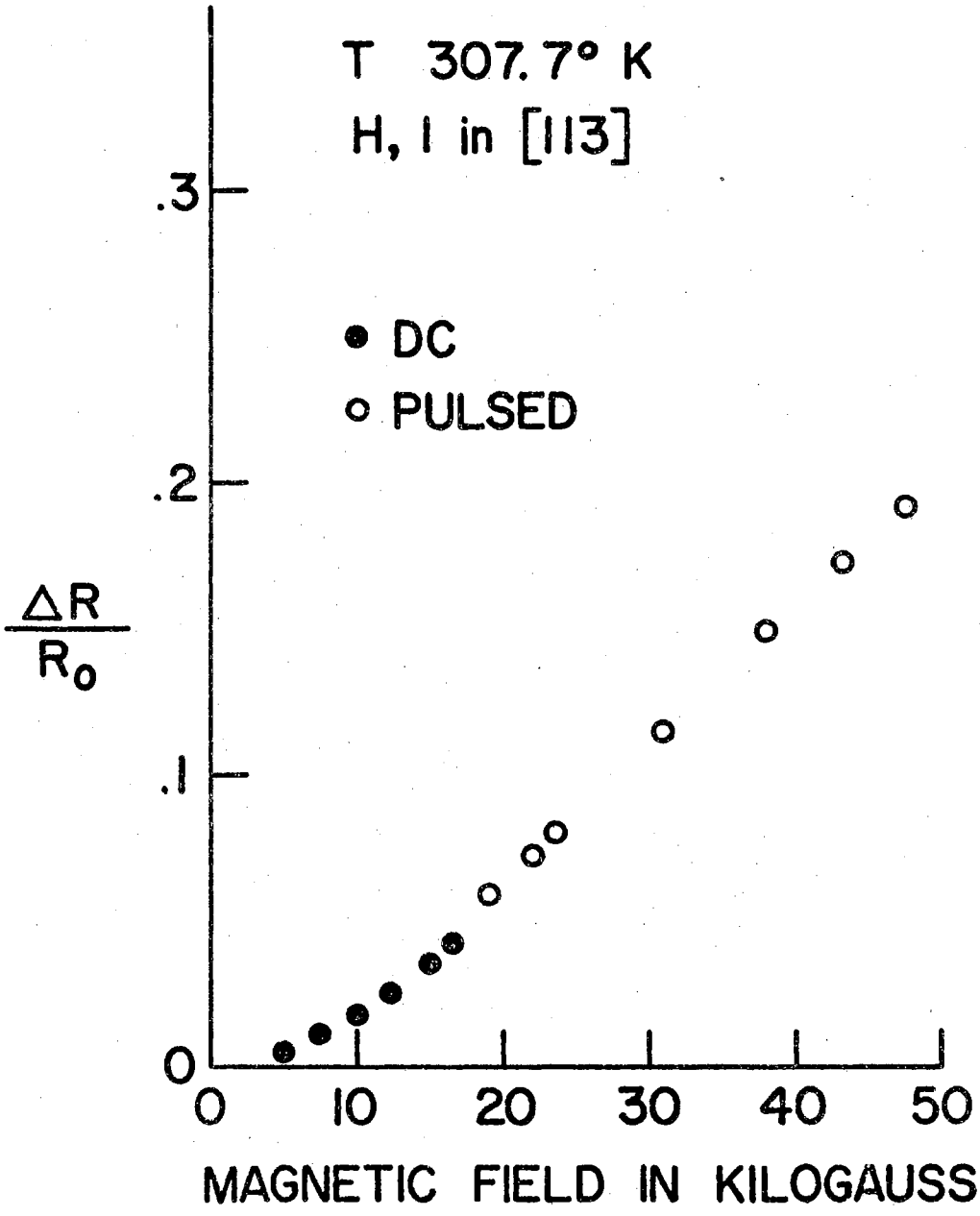

Fig. 22 Longitudinal Magnetoresistance in the [113] Direction for Low Magnetic Fields

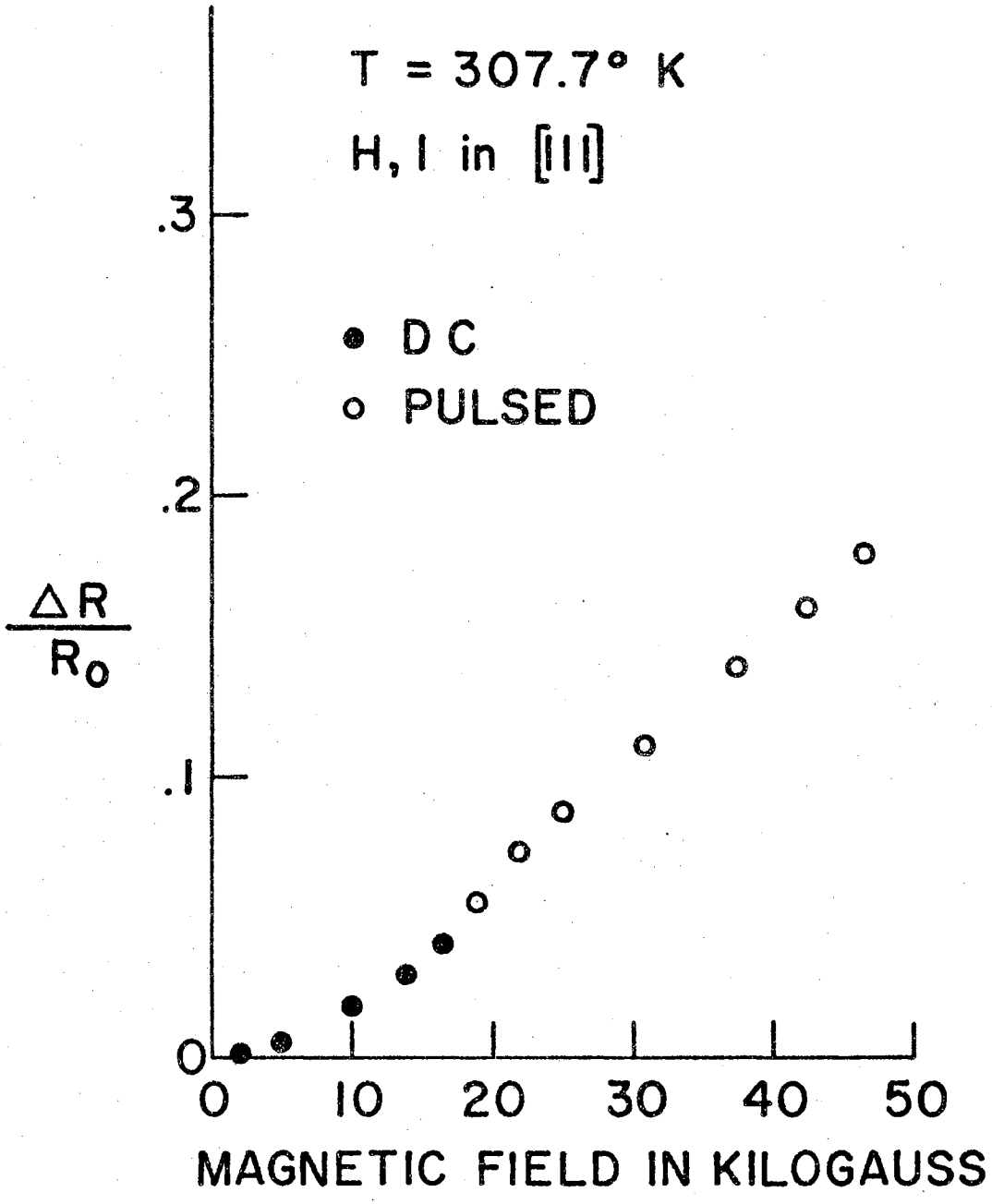

Fig. 23 Longitudinal Magnetoresistance in the [111] Direction For Low Magnetic Fields

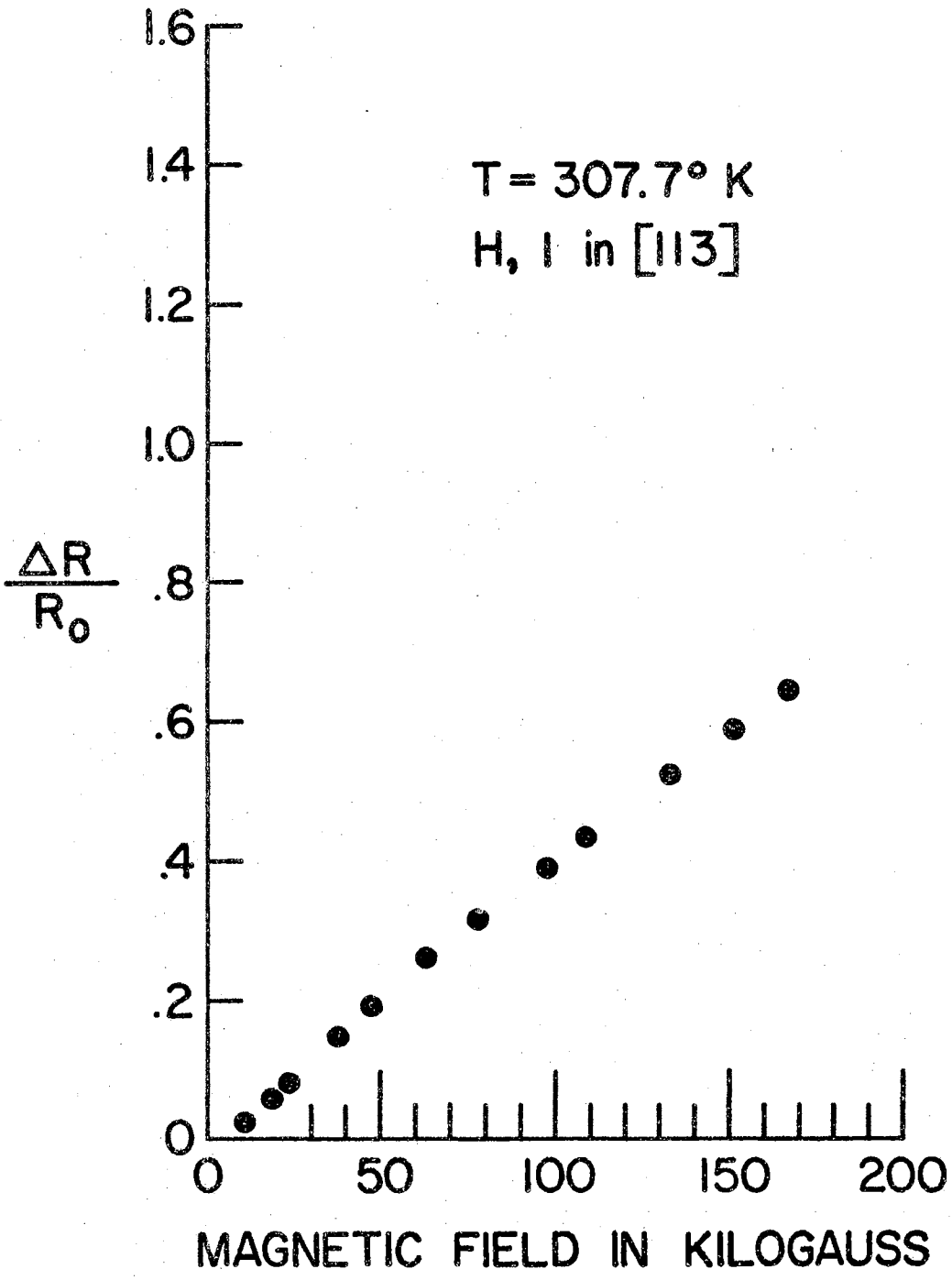

Fig. 24 Longitudinal Magnetoresistance in the [113] Direction

coil magnet which reliably produced magnetic fields on the order of 320 kilogauss, but trouble was experienced in keeping the leads in contact with the titanium hydride contacts at these magnetic fields.

Figure 25 is a graph of longitudinal magnetoresistance data in the [111] direction. The magnetic fields for these measurements were furnished by the pulsed magnet system. The points in Fig. 25 were obtained from three sets of magnetoresistance versus magnetic field data with the largest peak magnetic field being 167.8 kilogauss. Examination of Fig. 24 and Fig. 25 shows that the longitudinal magnetoresistances in the [111] and [113] directions become approximately the same at low magnetic fields.

Transverse Magnetoresistance

Transverse magnetoresistance effects were investigated with the use of both the dc magnet and the pulsed magnet system as described in Chapter IV. Transverse magnetoresistance was obtained for the current, I, in the [113] direction (current contacts on the (113) faces) with H in the [110] and in the [111] directions, and also for I in the [111] direction (current contacts on the (111) faces) with H in the [110] and in the [113] directions. The temperature of the sample was held at 307.7^{O}K during the measurements. Magnetoresistance measurements were somewhat less noisy when the current contacts were on (113) faces than when they were on (111) faces; this was probably due to the lower resistance between the potential probe contacts used when the current contacts were on the (113) faces.

Figure 26 is a graph of the transverse magnetoresistance with I in

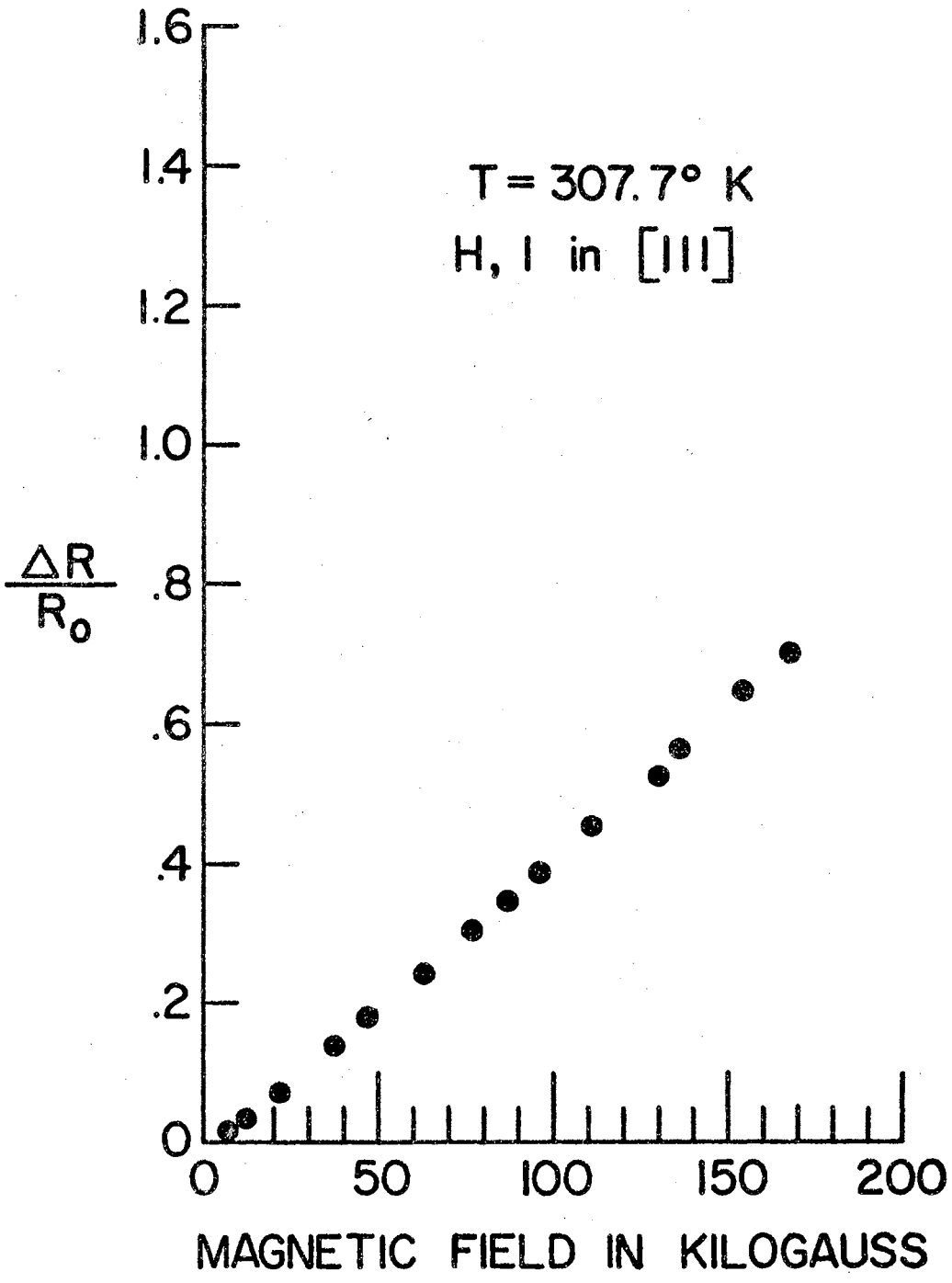

Fig. 25 Longitudinal Magnetoresistance in the [111] Direction

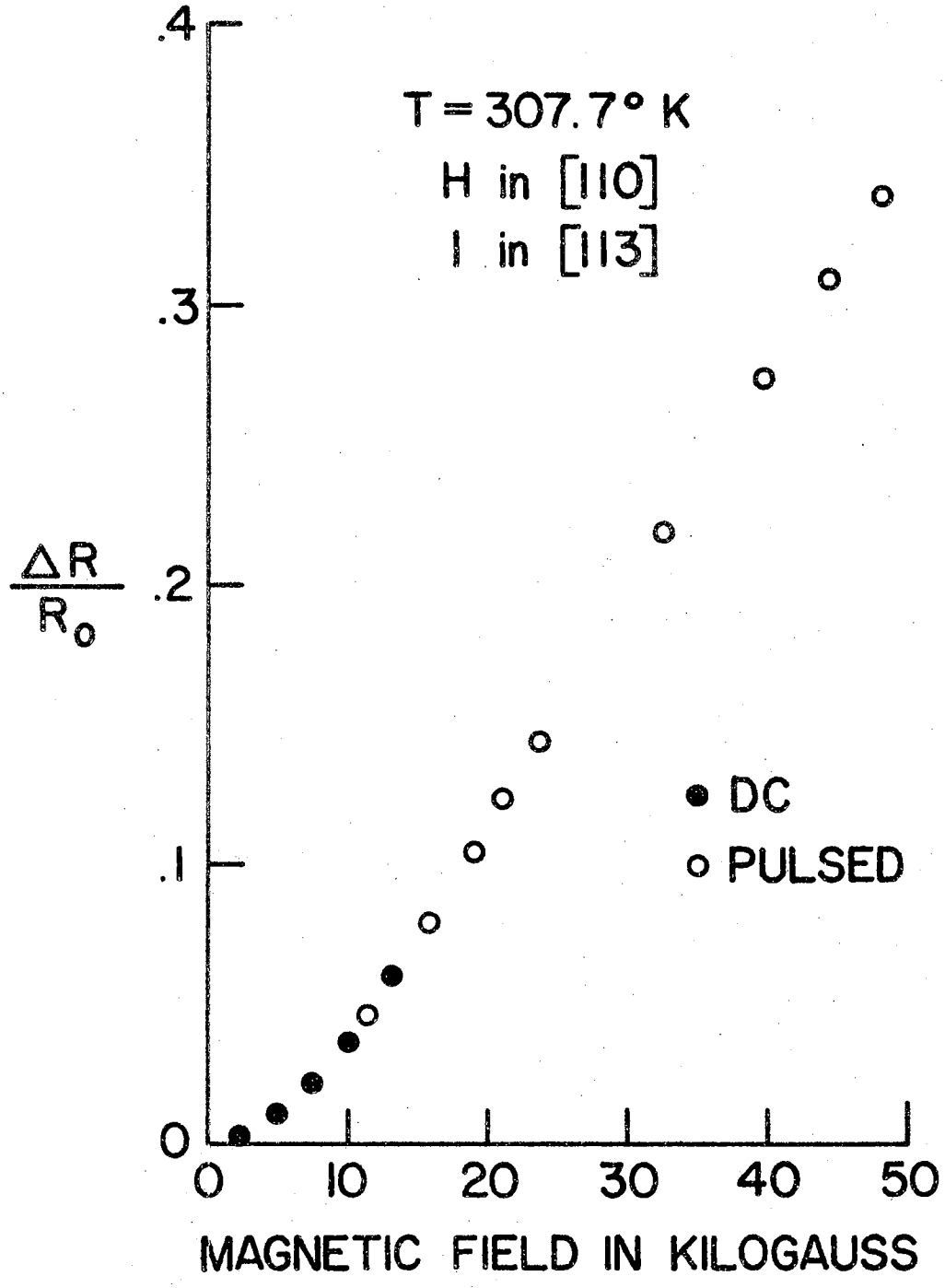

Fig. 26 Transverse Magnetoresistance with H in the [110] and I in the [113] Directions for Low Magnetic Fields

the [113] direction and H in the [110] direction for low magnetic fields. The experimental points represented by dots were obtained using the dc magnet, and the points represented by circles were obtained from two sets of magnetoresistance versus magnetic field data taken using the pulsed magnet system at two different peak magnetic fields. The agreement between the two sets of data taken with the pulsed magnet and with the data taken with the dc magnet is seen to be excellent.

Transverse magnetoresistance for I in the [111] direction and H in the [110] direction for low magnetic fields is shown in Fig. 27. The experimental points represented by dots were obtained using the dc magnet, and the points represented by circles were obtained from data taken with the pulsed magnet. The data taken with the pulsed magnet is seen to agree closely with that measured using the dc magnet.

A graph of the transverse magnetoresistance with I in the [113] direction and H in the [110] direction for both low and high magnetic fields is shown in Fig. 28. The data shown in Fig. 28 were observed using the pulsed magnet system to furnish the magnetic field. The points plotted in Fig. 28 were taken from four sets of magnetoresistance versus magnetic field data obtained using different peak magnetic fields (the peak magnetic fields ranged from 23.2 kilogauss to 165 kilogauss). Figure 28 illustrates good agreement between the four sets of magnetoresistance versus magnetic field data. The ratio of the longitudinal magnetoresistance in the [113] direction to the transverse magnetoresistance for I in the [113] direction and H in the [110] direction is .56 for a magnetic field of 165 kilogauss.

Transverse magnetoresistance for both low and high magnetic fields with I in the [111] direction and H in the [110] direction is shown in

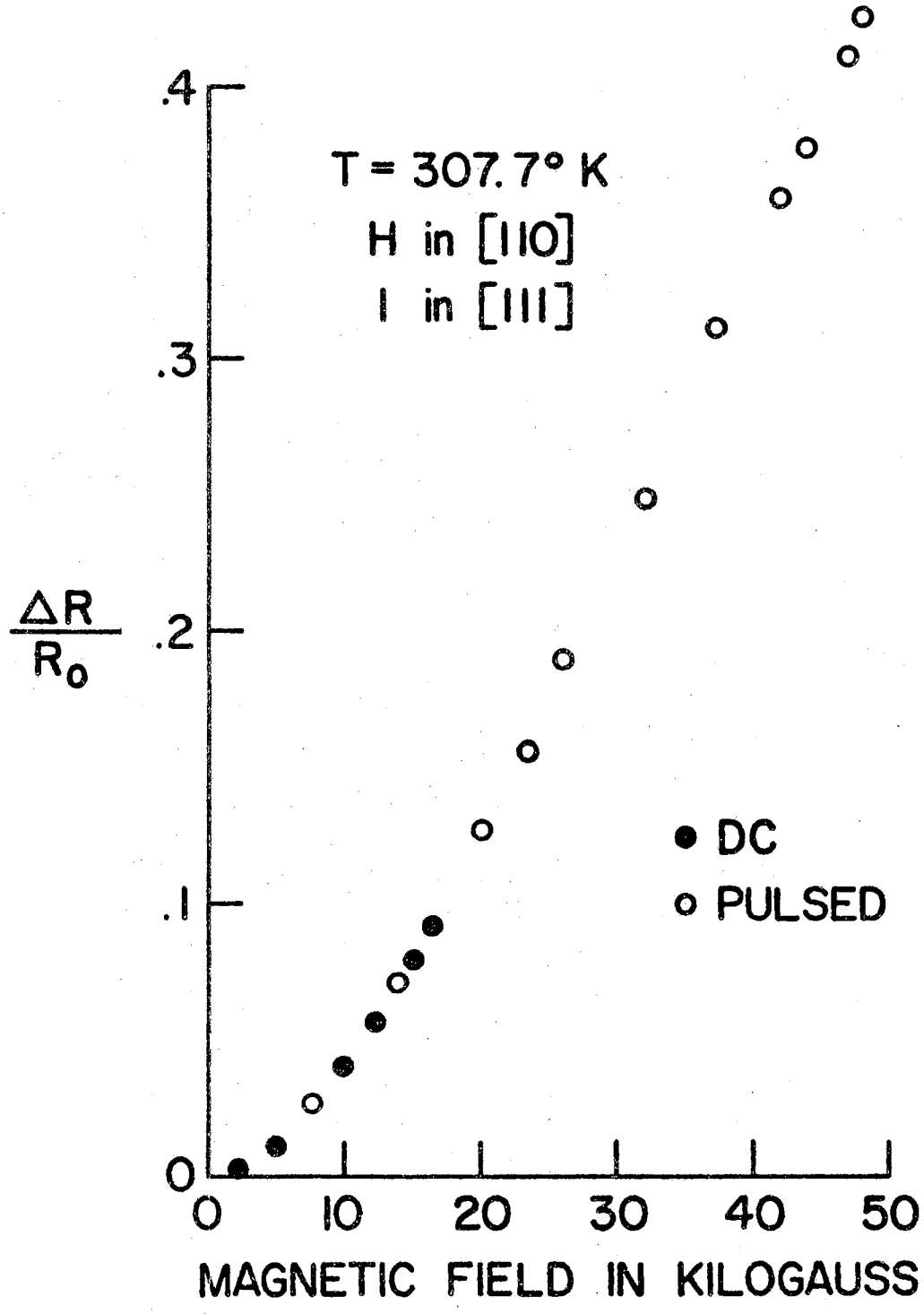

Fig. 27 Transverse Magnetoresistance with H in the [110] and I in the [111] Directions for Low Magnetic Fields

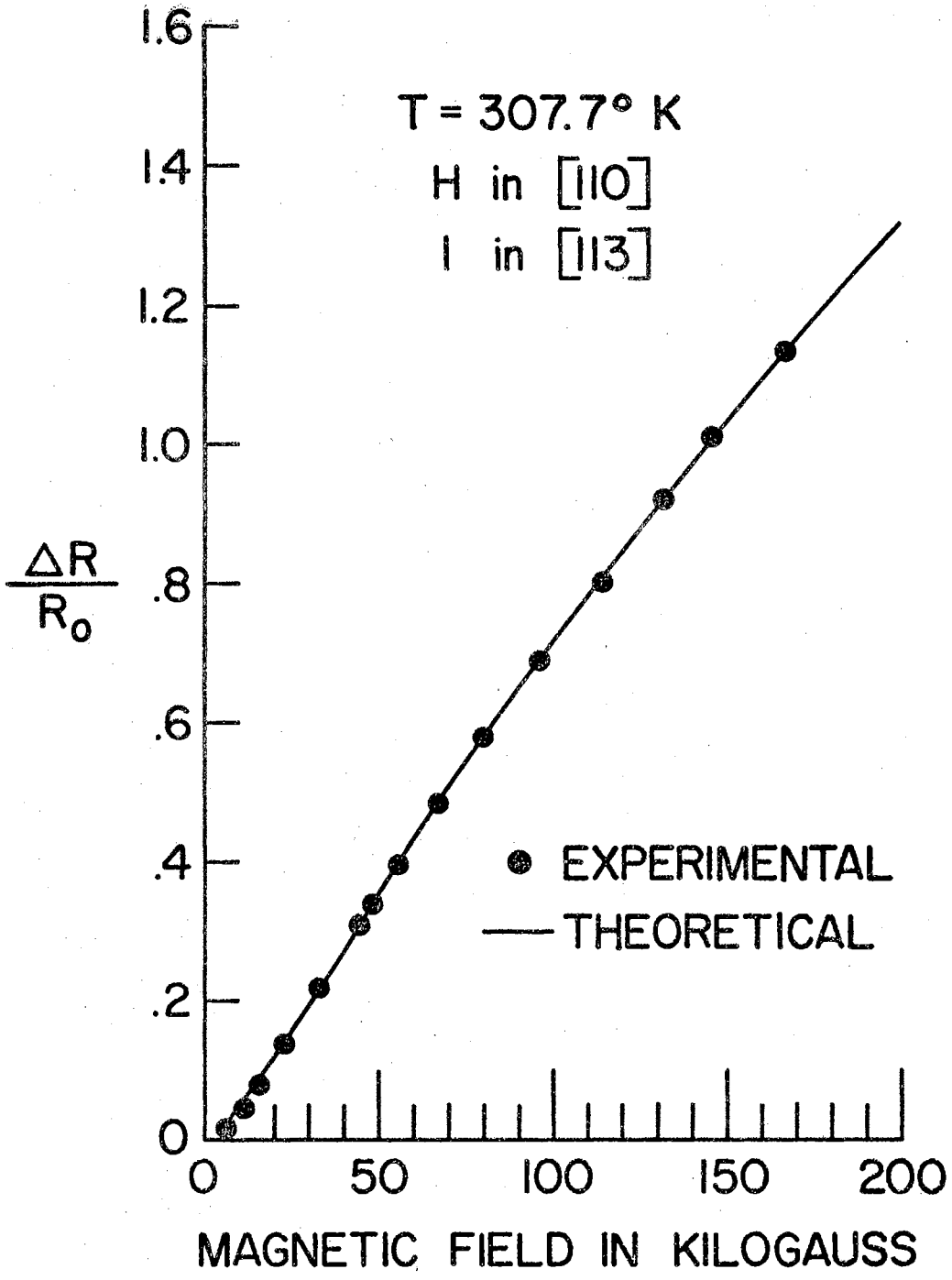

Fig. 28 Transverse Magnetoresistance with H in the [110] and I in the [113] Directions

Fig. 29. The pulsed magnet system was used to furnish the magnetic field. The data points were selected from three sets of magnetoresistance versus magnetic field data obtained using three different peak magnetic fields (up to 169 kilogauss). Agreement between the three sets of points is good. On comparing the transverse magnetoresistance at 165 kilogauss illustrated in Fig. 29 with that in Fig. 28 we find that the transverse magnetoresistance for I in the [111] direction and H in the [110] direction is approximately 3/2 times the transverse magnetoresistance for I in the [113] direction and H in the [110] direction. Also the ratio of longitudinal magnetoresistance in the [111] direction to the transverse magnetoresistance for I in the [111] direction and H in the (110) direction is approximately .4 at 165 kilogauss.

Figure 30 is a graph of transverse magnetoresistance for I in the [113] direction and H in the [111] direction measured at both low and high magnetic fields. As before, the data points were obtained from three sets of magnetoresistance versus magnetic field data using the pulsed magnet. Here also the agreement between the three sets of points is good. The transverse magnetoresistance in this orientation is approximately the same as that for transverse magnetoresistance with I in the [113] direction and H in the [110] direction.

A graph of transverse magnetoresistance with I in the [111] direction and H in the [113] direction for both low and high magnetic fields is shown in Fig. 31. Here too, the data points were obtained from three sets of magnetoresistance versus magnetic field measurements using the pulsed magnet system to furnish the magnetic field. In this case the agreement between the three sets of magnetoresistance versus magnetic

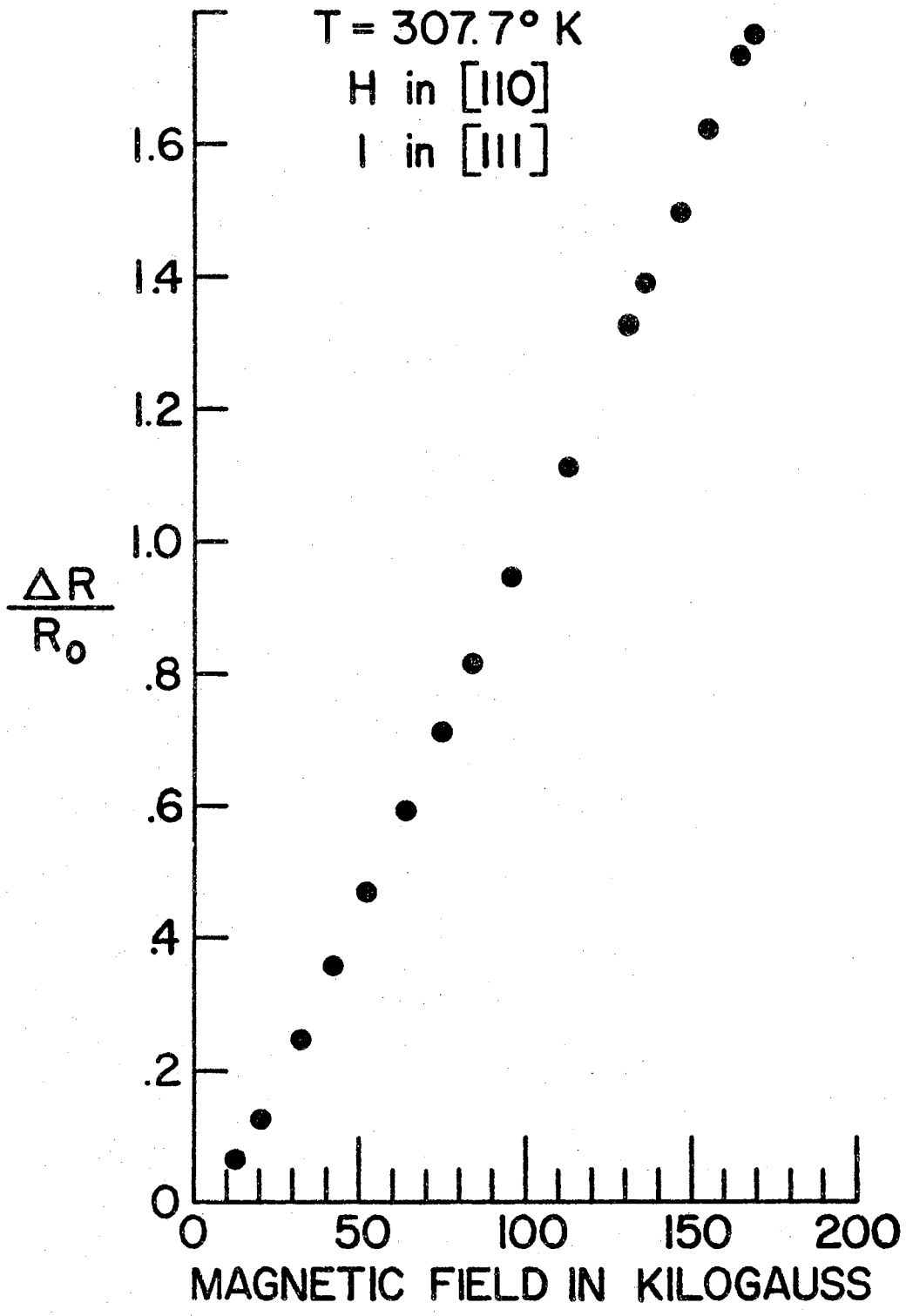

Fig. 29 Transverse Magnetoresistance with H in the [110] and I in the [111] Directions

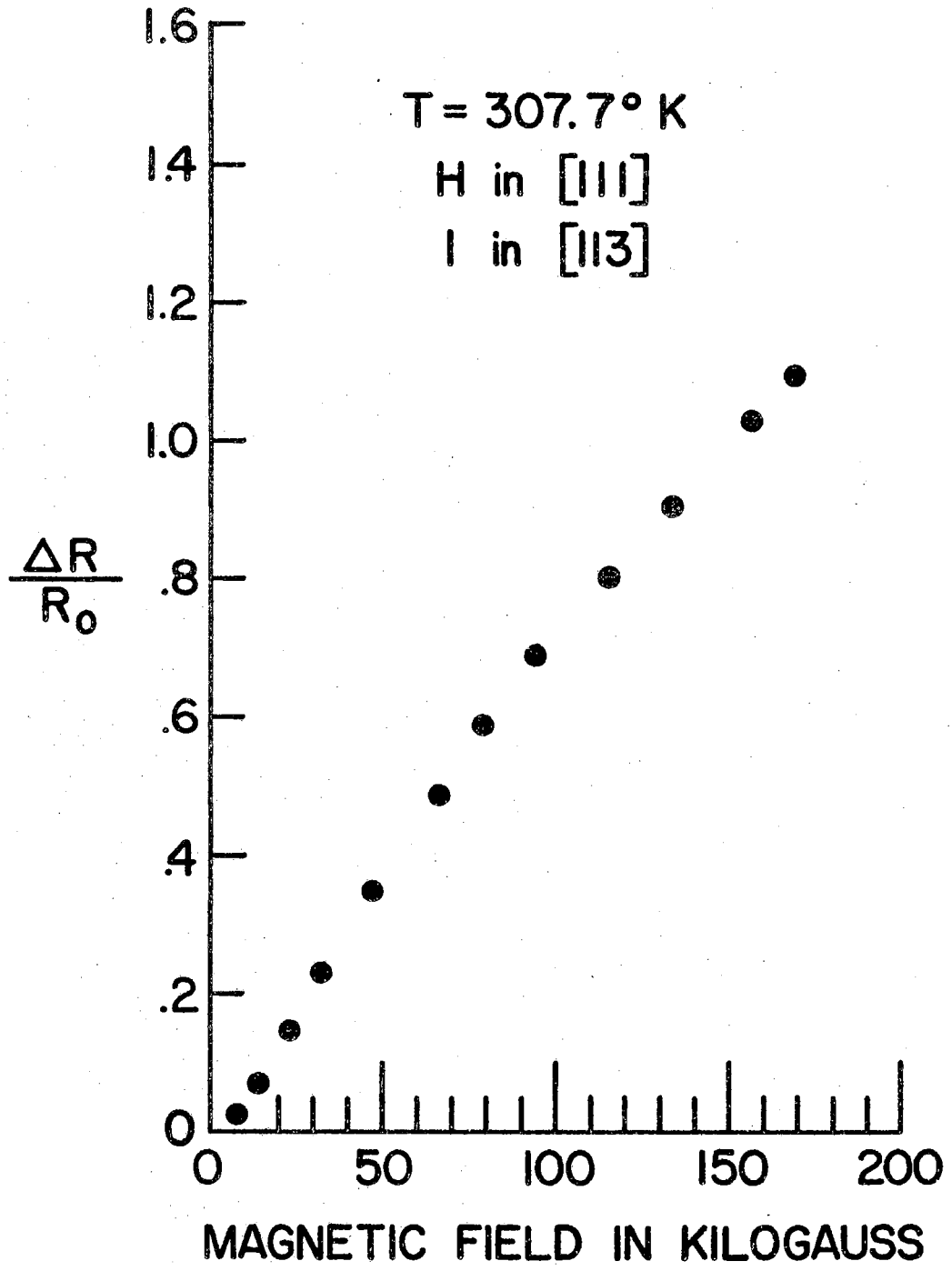

Fig. 30 Transverse Magnetoresistance with H in the [111] and I in the [113] Directions

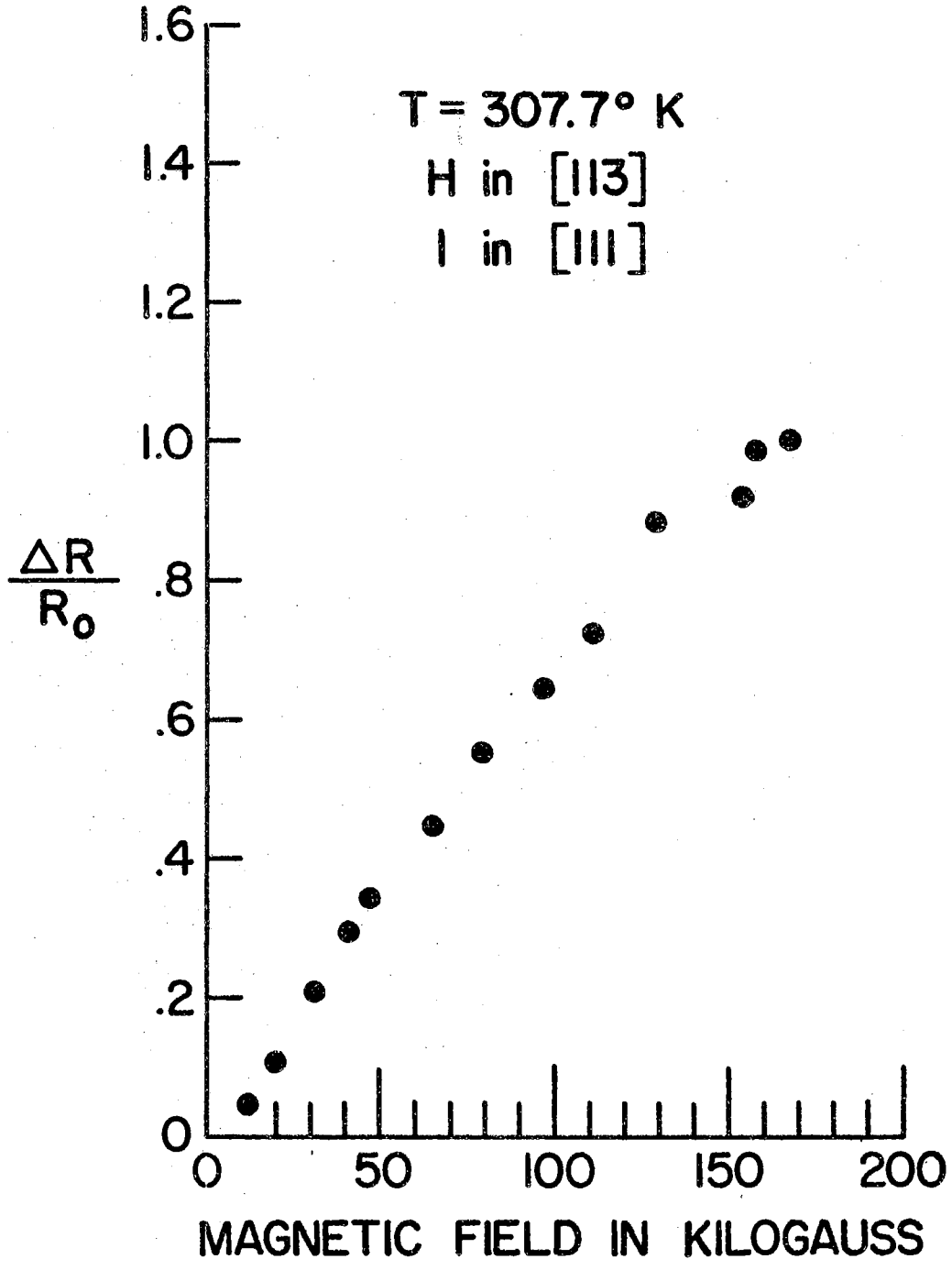

Fig. 31 Transverse Magnetoresistance with H in the [113] and I in the [111] Directions

field data is not as good as before which is due in part to the fact that the data obtained using the largest peak magnetic field, 167.8 kilogauss, were very noisy. Points obtained using peak magnetic fields lower than the largest peak magnetic field, and some of the points from the data obtained with the largest peak magnetic field, tend to indicate that the transverse magnetoresistance for I in the [111] direction and H in the [113] direction should be approximately the same as the transverse magnetoresistance for I in the [113] direction and H in the [111] direction. Comparing all of the cases of transverse magnetoresistance measured indicates all of the transverse magnetoresistances are approximately the same below about 15 kilogauss. Thus, at least for the cases investigated, the transverse magnetoresistance seems to be isotropic below this field.

CHAPTER VI

INTERPRETATION OF RESULTS

The results of the transverse magnetoresistance measurements were compared with the transverse magnetoresistance predicted by theory based on a particular model. The model assumes that the sample is a homogeneous, isotropic and isothermal solid. Mixed scattering (scattering by thermal lattice vibrations and scattering by ionized impurities) of the charge carriers where the process can be represented by a relaxation time is assumed. The conduction is assumed to be due to carriers from three uncoupled valence bands, and these bands are assumed to be associated with spherical energy surfaces. The effective masses of the holes in the three valance bands are taken to be $m^* = .7m_o$, $m^* = 1.06m_o$ and $m^* = 2.12m_o$ as determined by Rauch (25), where m_o is the mass of a free electron. The holes with effective masses $.7m_o$ and $2.12m_o$ are assumed to belong to the two valence bands that are degenerate at the center of the zone. The hole with effective mass $1.06m_o$ is assumed to belong to the band whose degeneracy at the center of the zone is removed by inclusion of spin-orbit interaction. This band will be called the split-off band and the spin-orbit splitting will be taken as .006 electron volts (25).

Development of Equations

For isotropic systems and the magnetic field H in the z-direction, Beer (26) has shown the transverse magnetoresistance may be written for

a single band in terms of the components, $S_{xx}(H)$ and $S_{xy}(H)$, of the conductivity tensor as

$$\frac{\Delta\rho}{\rho_o} = \frac{S_{xx}(H)S_{xx}(0)}{S_{xx}^2(H) + S_{xy}^2(H)} - 1. \tag{6-1}$$

For an isotropic solid in which three bands are important the tensor components $S_{xx}(H)$ and $S_{xy}(H)$ are redefined in terms of the components of the conductivity of each band (26). Thus for the case of three valence bands

$$\begin{aligned} S_{xx}(H) &= {}_1\sigma_{xx}(H) + {}_2\sigma_{xx}(H) + {}_3\sigma_{xx}(H) \\ S_{xy}(H) &= {}_1\sigma_{xy}(H) + {}_2\sigma_{xy}(H) + {}_3\sigma_{xy}(H). \end{aligned} \tag{6-2}$$

The subscript 1 will denote the light hole band, the subscript 2 will denote the heavy hole band and the subscript 3 will denote the split-off band.

The components, $\sigma_{xx}(H)$, $\sigma_{xy}(H)$ and $\sigma_{zz}(H)$, of the conductivity tensor for a single band and for the magnetic field in the z-direction may be written in the form

$$\begin{aligned} \sigma_{xx}(H) &= -\frac{e^2}{4\pi^3\hbar^2}\int \frac{\tau\left(\frac{\partial E}{\partial k_x}\right)^2}{1 + (\omega\tau)^2}\frac{\partial f_o}{\partial E}\, d^3k \\ \sigma_{xy}(H) &= \frac{e^2}{4\pi^3\hbar^2}\int \frac{\omega\tau^2\left(\frac{\partial E}{\partial k_x}\right)^2}{1 + (\omega\tau)^2}\frac{\partial f_o}{\partial E}\, d^3k \\ \sigma_{zz}(H) &= -\frac{e^2}{4\pi^3\hbar^2}\int \tau\left(\frac{\partial E}{\partial k_z}\right)^2\frac{\partial f_o}{\partial E}\, d^3k. \end{aligned} \tag{6-3}$$

where $\omega = eH/m^*c$, τ is the relaxation time, f_o is the equilibrium distribution function for holes and E is the energy (26). Since the longitudinal magnetoresistance for a single band may be written as

$$\frac{\Delta\rho}{\rho_o} = \frac{\sigma_{zz}(0)}{\sigma_{zz}(H)} - 1 \tag{6-4}$$

the preceeding expression for $\sigma_{zz}(H)$ shows that the longitudinal magnetoresistance in an isotropic solid is zero. Assuming Maxwell-Boltzmann statistics, which are applicable here, and spherical energy surfaces the expressions for $\sigma_{xx}(H)$ and $\sigma_{xy}(H)$ may be put in the form

$$\sigma_{xx} = \frac{4pe^2}{3\pi^{\frac{1}{2}}m^*} \int_o^\infty \frac{\tau}{1 + (\omega\tau)^2} \alpha^{3/2} e^{-\alpha} d\alpha \tag{6-5}$$

and

$$\sigma_{xy} = -\frac{4pe^2}{3\pi^{\frac{1}{2}}m^*} \int_o^\infty \frac{\omega\tau^2}{1 + (\omega\tau)^2} \alpha^{3/2} e^{-\alpha} d\alpha \tag{6-6}$$

where $\alpha = \frac{E_v - E}{kT}$ and

$$p = \tfrac{1}{4} \left(\frac{2m^*kT}{\pi\hbar^2}\right)^{3/2} e^{\frac{E_v - E_F}{kt}} \tag{6-7}$$

is the hole density and $e < 0$ for electrons. The relaxation time, τ, for the case of mixed scattering by lattice vibrations and ionized impurities may be written, following Beer and Willardson (27),

$$\tau = \frac{3\pi^{\frac{1}{2}}}{4} \frac{m^*}{e} \mu_L \frac{\alpha^{3/2}}{\beta + \alpha^2} \tag{6-8}$$

where μ_L is the lattice scattering mobility for a spherical band and β is a slowly varying function of energy that is chosen constant throughout an integration and which has been approximated as $\beta = 6(\mu_L/\mu_I)$ by others; μ_I

is the ionized impurity scattering mobility. The magnitude of β gives an indication of the degree of impurity scattering. The expressions for the conductivity coefficients $\sigma_{xx}(H)$ and $\sigma_{xy}(H)$ using the above expression for τ are

$$\sigma_{xx}(H) = pe\mu_L K(\beta,\gamma) \tag{6-9}$$

and

$$\sigma_{xy} = -\frac{\pi^{\frac{1}{2}}}{2} pe\mu_L \gamma^{\frac{1}{2}} L(\beta,\gamma) \tag{6-10}$$

where $K(\beta,\gamma)$ and $L(\beta,\gamma)$ are the integrals

$$K(\beta,\gamma) = \int_0^\infty \frac{\alpha^3 e^{-\alpha}(\alpha^2+\beta)}{(\alpha^2+\beta)^2+\gamma\alpha^3}\, d\alpha \tag{6-11}$$

$$L(\beta,\gamma) = \frac{2}{\pi^{\frac{1}{2}}} \int_0^\infty \frac{\alpha^{9/2} e^{-\alpha}}{(\alpha^2+\beta)^2+\gamma\alpha^3}\, d\alpha \tag{6-12}$$

and

$$\gamma = \frac{9\pi}{16}\left(\frac{H\mu_L}{c}\right)^2.$$

The expressions (6-9) and (6-10) for the conductivity coefficients are then inserted in the equations (6-1) and (6-2) giving

$$\frac{\Delta\rho}{\rho_o} = \frac{A(\beta,\gamma)A(\beta,0)}{[A(\beta,\gamma)]^2 + B(\beta,\gamma)} - 1 \tag{6-13}$$

where

$$A(\beta,\gamma) = \frac{p_1}{p_2}\frac{\mu_{L,1}}{\mu_{L,2}} K(\beta_1,\gamma_1) + K(\beta_2,\gamma_2) + \frac{p_3}{p_2}\frac{\mu_{L,3}}{\mu_{L,2}} K(\beta_3,\gamma_3) \tag{6-14}$$

and

$$B(\beta,\gamma) = \frac{\pi}{4}\gamma_2\left[\frac{p_1}{p_2}\left(\frac{\mu_{L,1}}{\mu_{L,2}}\right)^2 L(\beta_1,\gamma_1) + L(\beta_2,\gamma_2) + \frac{p_3}{p_2}\left(\frac{\mu_{L,3}}{\mu_{L,2}}\right)^2 L(\beta_3,\gamma_3)\right]^2 \tag{6-15}$$

for the transverse magnetoresistance.

Application to Experimental Results

In applying equation (6-13) to the experimental results the ratios of the hole densities p_1/p_2 and p_3/p_2, the ratio of the lattice scattering mobilities $\mu_{L,1}/\mu_{L,2}$ and $\mu_{L,3}/\mu_{L,2}$, and the ratios of the β's, β_1/β_2 and β_3/β_2, were calculated from expressions developed assuming spherical energy surfaces and specific models of scattering. Obviously once the ratios of the scattering mobilities are known the ratios of the γ's, γ_1/γ_2 and γ_3/γ_2, for a particular magnetic field are also known. Also the expression for γ in laboratory units where μ_L is in cm^2/volt-sec. and H is in gauss is

$$\gamma = \frac{9\pi}{16}\left(\frac{\mu_L H}{10^8}\right)^2 \tag{6-16}$$

From (6-7) an estimate of the ratios of the hole densities can be calculated. Since E_v is the same for bands 1 and 2 the ratio p_1/p_2 is

$$\frac{p_1}{p_2} = \left(\frac{m^*_1}{m^*_2}\right)^{3/2} = .19 \tag{6-17}$$

Since the top of band 3 is assumed to be .006 electron volts below the bands 1 and 2, i.e., at E_v - .006, the ratio of p_3/p_2 can be written

$$\frac{p_3}{p_2} = \left(\frac{m^*_3}{m^*_2}\right)^{3/2} e^{-\frac{.006}{kT}} = .28 \tag{6-18}$$

where kT is evaluated at T = 307.7°K. According to Beer (26) the lattice scattering mobilities have mass dependencies of $(m^*)^{-5/2}$. Thus the ratios of the mobilities are given by

$$\frac{\mu_{L,1}}{\mu_{L,2}} = \left(\frac{m^*_2}{m^*_1}\right)^{5/2} = 15.6 \qquad (6\text{-}19)$$

$$\frac{\mu_{L,3}}{\mu_{L,2}} = \left(\frac{m^*_2}{m^*_3}\right)^{5/2} = 5.66 \qquad (6\text{-}20)$$

Also the ionized impurity scattering mobilities have mass dependencies of $(m^*)^{-\frac{1}{2}}$. Then approximating β by $6\mu_L/\mu_I$ the ratios of the β's are

$$\frac{\beta_1}{\beta_2} = \left(\frac{m^*_2}{m^*_1}\right)^2 = 9 \qquad (6\text{-}21)$$

$$\frac{\beta_3}{\beta_2} = \left(\frac{m^*_2}{m^*_3}\right)^2 = 4 \qquad (6\text{-}22)$$

The integrals $K(\beta,\gamma)$ and $L(\beta,\gamma)$ can be evaluated numerically and are tabulated elsewhere (29). The integral $K(\beta,0)$ may be expressed as

$$K(\beta,0) = 1 + \beta[\cos \beta^{\frac{1}{2}}\mathrm{Ci}\beta^{\frac{1}{2}} + \sin \beta^{\frac{1}{2}}(\mathrm{Si}\beta^{\frac{1}{2}} - \tfrac{\pi}{2})] \qquad (6\text{-}23)$$

where Ci x and Si x are the cosine and sine integrals respectively and are tabulated by Jahnke and Emde (30). The ratios of the carrier densities p_1/p_2 and p_3/p_2 and the ratios of the β's were held constant and the magnitude of the β's, the lattice scattering mobility $\mu_{L,2}$ and the ratios of the lattice scattering mobilities were varied to give the best fit of the predicted transverse magnetoresistance curve to the data points due to

the transverse magnetoresistance for H in the [110] direction and I in the [113] direction illustrated in Fig. 28. The predicted transverse magnetoresistance curve is also shown in Fig. 28. The values of the parameters for this best fit were $\beta_2 = .0001$, $\beta_1 = .001$, $\beta_3 = .0003$, $\mu_{L,1}/\mu_{L,2} = 20$, $\mu_{L,3}/\mu_{L,2} = 7$ and $\mu_{L,2} = 195$ cm^2/volt-sec.

Summary and Conclusion

Transverse and longitudinal magnetoresistance was measured for several orientations in semiconducting diamond at magnetic fields up to approximately 170 kilogauss. Longitudinal magnetoresistance was measured in the [113] and [111] directions. Transverse magnetoresistance was measured with the current, I, in the [113] direction and H in the [110] and [111] directions and with I in the [111] direction and H in the [110] and [113] directions. Assuming a model in which the conduction is due to holes from three uncoupled valence bands characterized by spherical energy surfaces, mixed scattering by lattice vibrations and ionized impurities is applicable, and the sample is an isothermal isotropic solid, the theoretical magnetoresistance was calculated and parameters in the equation were adjusted to give the best fit to experimental transverse magnetoresistance for I in the [113] and H in the [110] direction. The values of the parameters that gave the best fit can be used to calculate the corresponding values of the carrier densities, the lattice scattering hole mobilities, and the β's for each band. The results are shown in Table II.

The conductivity mobility, μ, defined by the equation

$$\sigma(H) = pe\mu \qquad (6\text{-}24)$$

TABLE II

PARAMETERS FOR BEST FIT

	Light Hole Band (Band 1)	Heavy Hole Band (Band 2)	Split-off Band (Band 3)
Carrier Density	$.19p_2$	p_2	$.28p_2$
Lattice Scattering Hole Mobility (cm^2/volt-sec)	3900	195	1365
β	.001	.0001	.0003

may be expressed in terms of the conductivity mobilities μ_1, μ_2, and μ_3 of each band by the equation

$$\mu = \frac{P_1\mu_1 + P_2\mu_2 + P_3\mu_3}{P_1 + P_2 + P_3} \tag{6-25}$$

The mobilities μ_1, μ_2, and μ_3 have in turn been shown to be given by

$$\mu_i = \mu_{L,i} K(\beta,0) \qquad i = 1,2,3 \tag{6-26}$$

in the zero magnetic field limit (26). If we assume this relation to hold for the magnetic fields used in this experiment the conductivity mobility thus evaluated is μ = 900 cm^2/volt-sec. The Hall mobility was measured in this diamond to be 1300 cm^2/volt-sec by Leivo et al. (24).

During the course of this investigation many improvements and problems deserving further study presented themselves. The most obvious extension of the work is to try to analyze the data using a suitable theory that takes into account the anisotropy of the crystal and explains the longitudinal magnetoresistance effects. The theory presented here cannot, as illustrated earlier, predict the observed longitudinal magnetoresistance and assumes the material to be isotropic. Most theories of anisotropic materials assume one of two limiting cases, either very weak or very strong magnetic fields. Analysis of magnetoresistance data for diamond has been done for weak fields (12, 13, 15, 16). Application of very strong magnetic field theory is hampered by the magnitude of the magnetic field needed to achieve saturation of the magnetoresistance. The method developed by McClure (19) is applicable to magnetoresistance in arbitrary magnetic fields for general band structures in the case where an energy dependent relaxation time may be used. However the analytical determination of the Fourier components of the velocity needed to evaluate the magnetoresistance using this theory is very tedious. Thus most evaluations

using this method have involved special simplifying assumptions as to the shape of the energy surfaces, and such a method may be applicable here (27, 31). The method of McClure (19) is still not expected to be able to explain the difference in the transverse magnetoresistances shown in Figs. 28 and 29. Therefore work along the line of producing a more general theory of the magnetoresistance effect in materials is needed. In evaluating equations for magnetoresistance such as (6-13) which involve a number of parameters programming the problem on a computer should allow much greater precision in fitting a theoretical curve to particular data. In the realm of further experimentation on diamond, obviously similar measurements on another semiconducting diamond with the same orientation as the present sample are desirable to see if the data are repeatable for different semiconducting diamonds. In particular a more homogeneous diamond sample is needed. Measurements of the magnetoresistance in other orientations, especially with the magnetic field in the [100] direction, are desirable since they may be easier to treat using the method of McClure (19). The peak magnetic field usable in the magnetoresistance measurements probably can be increased as soon as a new technique for fastening the electrical leads to the titanium hydride contacts on the diamond is developed. Magnetoresistance at magnetic fields approximately two times the magnitude used here probably will begin to approach saturation for some directions in the sample such as for H in the [110] and I in the [113] directions. Such data should allow one to choose the parameters involved in equation (6-13) with greater precision. Also, work in the allied field of the Hall effect in diamond for arbitrary magnetic fields would be useful in explaining the observed effects. Finally, a theoretical determination of the lattice

scattering mobility for holes in diamond could be carried out similar to the analysis by Tiersten (32).

BIBLIOGRAPHY

1. Adams, E. N. and Keyes, R. W. "Galvanomagnetic Phenomena in Very Strong Magnetic Fields" Progress in Semiconductors, Volume 6, Ed. Alan F. Gibson. New York: John Wiley and Sons, Inc., 1962, pp. 87 to 142.

2. Drabble, J. R. and Wolfe, R. "Geometrical Effects in Transverse Magnetoresistance Measurements" J. Elec. and Control 3, 259 (1957).

3. Thomson, Sir Wm. "On the Effects of Magnetization on the Electrical Conductivity of Metals" Phil. Trans. 146, 736 (1856).

4. Neesen, F. "Ueber den Einfluss der Magnetisierung auf den Leitungswiderstand Magnetischer Flüssigkeiten" Wied. Ann. 23, 482 (1884).

5. Boltzman, L. "Ueber die Wirkung des Magnetismus auf Elektrische Entladungen in Verdünnten Gasen" Phil. Mag. 24, 373 (1887).

6. Drude, P. and Nernst, W. "Einfluss der Temperatur und des Aggregatzustands auf das Verhalten des Wismuths im Magnetfelde" Wied. Ann. 42, 568 (1891).

7. Wilson, H. A. "Effect of a Magnetic Field on the Electrical Conductivity of Flames" Proc. Roy. Soc. (London) A82, 595 (1909).

8. Laws, S. C. "The Change of Resistance of Metals in a Magnetic Field at Different Temperatures" Phil. Mag. 19, 685 (1910).

9. Königsberger, J. and Gottstein, G. "Galvano- und thermomagnetische Effekte Variabler Leiter und Metalle" Ann. d. Phys. 46, 446 (1915).

10. Kapitza, P. "Further Developments of the Method of Obtaining Strong Magnetic Fields" Proc. Roy. Soc. A115, 658 (1927).

11. Campbell, L. L. Galvanomagnetic and Thermomagnetic Effects; The Hall and Allied Phenomena. New York: Longmans, Green and Co., 1923.

12. Wedepohl, P. T. "Electrical and Optical Properties of Type IIb Diamonds" Proc. Phys. Soc. (London) B70, 177 (1957).

13. Mitchell, E. W. J. and Wedepohl, P. T. "Magnetoresistance of a Type IIb Semiconducting Diamond" Proc. Phys. Soc. (London) B70, 527 (1957).

14. Pearson, G. L. and Suhl, H. "The Magneto-resistance Effect in Oriented Single Crystals of Germanium" Phys. Rev. 83, 768 (1951).

15. Bate, R. T. and Willardson, R. K. "Hall Coefficient and Magneto-resistance of Semiconducting Diamond" Tech. Document AFOSR-TN-58-916.

16. Kemmey, P. J. and Mitchell, E. W. J. "The Magneto-resistance of p-type Semiconducting Diamond" Proc. Roy. Soc. (London) 263, 420 (1961).

17. Furth, H. P. and Waniek, R. W. "High-Field Longitudinal Magneto-resistance of Germanium" Phys. Rev. 104, 343 (1956).

18. Champness, C. H. "High-Field Magnetoresistance Measurements at Room Temperature in Indium Antimonide" High Magnetic Fields. Ed. Henry Kolm et al. New York: John Wiley and Sons, Inc., 1962, pp. 528 to 533.

19. McClure, J. W. "Field Dependence of Magnetoconductivity" Phys. Rev. 101, 1642 (1956).

20. Kondorskii, E. I. and Susov, E. V. "Apparatus for Generating Intense Magnetic Fields of Short Duration" Instruments and Experimental Techniques 1, 118 (1963).

21. Foner, S. and Kolm, H. "Coils for the Production of High-Intensity Pulsed Magnetic Fields" Rev. Sci. Instr. 28, 799 (1957).

22. Howland, B. and Foner, S. "Flux Concentration by Stationary Conductors" High Magnetic Fields. Ed Henry Kolm et al. New York: John Wiley and Sons, Inc., 1962, pp. 249 to 258.

23. Young, T. "The Hall Effect in Semiconducting Diamond" (Thesis, Oklahoma State University, August, 1958), ASTIA-AD-211 037.

24. Leivo, W. J., et al. "Investigation of Semiconducting Properties of Type IIb Diamonds" (Final Report, Air Force Office of Scientific Research, May 1962), AFOSR-2642.

25. Rauch, C. J. "Millimeter Cyclotron Resonance in Diamond" Proceedings of the International Conference on the Physics of Semiconductors, Exeter, July, 1962.

26. Beer, A. C. "Galvanomagnetic Effects in Semiconductors." Solid State Physics. Supplement 4. Ed. Frederick Seitz and David Turnbull. New York: Academic Press, 1963.

27. Beer, A. C. and Willardson, R. K. "Hall and Transverse Magneto-resistance Effects for Warped Bands and Mixed Scattering" Phys. Rev. 110, 1286 (1958).

28. Johnson, V. A. and Whitesell, W. J. "Theory of the Magnetoresistive Effect in Semiconductors" Phys. Rev. 89, 941 (1953).

29. Beer, A. C., Armstrong, J. A. and Greenberg, I. N. "Evaluation of Transport Integrals for Mixed Scattering and Application to Galvanomagnetic Effect" Phys. Rev. 107, 1506 (1957).

30. Jahnke, E. and Emde, F. Tables of Functions with Formulas and Curves. New York: Dover, 1943.

31. Goldberg, C., Adams, E. N. and Davis, R. E. "Magnetoconductivity in p-Type Germanium" Phys. Rev. 105, 865 (1957).

32. Tiersten, M. "Acoustic-Mode Scattering Mobility of Holes in Diamond Type Semiconductors" J. Phys. Chem. Solids 25, 1151 (1964).

VITA

Kenneth Jess Russell

Candidate for the Degree of

Doctor of Philosophy

Thesis: HIGH FIELD MAGNETORESISTANCE OF SEMICONDUCTING DIAMOND

Major Field: Physics

Biographical:

Personal Data: Born in Oklahoma City, Oklahoma, March 13, 1936, the son of Jess O. and Lily Mae Russell.

Education: Attended grade school at Oak Hill grade school in Noble County, Oklahoma; graduated from Perry High School in 1953; received the Bachelor of Science degree from the Oklahoma State University, with a major in Physics, in May, 1959; completed requirements for the Doctor of Philosophy degree in August, 1965.

Professional experience: Worked for one and one half years as a meter repairman for the Public Service Company of Oklahoma at Tulsa; worked one summer as a student engineer in the Servomechanisms Design Group for Chance Vought Aircraft at Dallas, Texas; since 1960 has been constructing apparatus and making studies of semiconductor phenomena, part of which are described in this thesis; is a member of Pi Mu Epsilon, Sigma Pi Sigma, and Phi Kappa Phi.